

Accepted Manuscript

A unified frequency domain fatigue damage modeling approach for random-on-random spectrum

Z. Li, A. Ince

PII: S0142-1123(19)30052-0
DOI: <https://doi.org/10.1016/j.ijfatigue.2019.02.032>
Reference: JIJF 4997

To appear in: *International Journal of Fatigue*

Received Date: 20 November 2018
Revised Date: 21 February 2019
Accepted Date: 22 February 2019

Please cite this article as: Li, Z., Ince, A., A unified frequency domain fatigue damage modeling approach for random-on-random spectrum, *International Journal of Fatigue* (2019), doi: <https://doi.org/10.1016/j.ijfatigue.2019.02.032>

This is a PDF file of an unedited manuscript that has been accepted for publication. As a service to our customers we are providing this early version of the manuscript. The manuscript will undergo copyediting, typesetting, and review of the resulting proof before it is published in its final form. Please note that during the production process errors may be discovered which could affect the content, and all legal disclaimers that apply to the journal pertain.



A unified frequency domain fatigue damage modeling approach for random-on-random spectrum

Z. Li¹, A. Ince^{1,2*}

¹Purdue Polytechnic Institute, Purdue University, West Lafayette, Indiana, USA

²Department of Mechanical, Industrial & Aerospace Engineering,
Concordia University, Montreal, Quebec, Canada

*Corresponding author: Phone: + 1 (514) 848 2424, e-mail:ayhan.ince@concordia.ca

Abstract

Current frequency domain damage models only deal with stationary random loadings (stationary Power Spectral Density), but many machine components, such as jet engines, rotating machines, and tracked vehicles are subjected to evolutionary i.e. time-dependent PSD conditions under real service loadings. An innovative fatigue damage modeling approach is proposed to predict fatigue damage of structures under complex evolutionary PSD loading conditions where the topology of PSD function changes with time. This new approach is based on a novel modeling framework that the evolutionary PSD response of a structure can be decomposed into a finite number of discrete PSD functions. Each PSD function can be split into narrow frequency bands so that each of narrowbands can be associated with Rayleigh distribution of stress cycles. Fatigue damage can then be predicted by summing up damages for each individual band and each discrete PSD function on the basis of a damage accumulation rule. The proposed modeling approach is numerically and experimentally validated by a finite element method and experiments. The proposed modeling approach provides a more efficient and accurate modeling technique for fatigue damage assessment of engineering structural components under very complex random loadings.

Keywords: Fatigue failure, accelerated test, power spectral density, frequency domain, random loading

Nomenclature

T_r	Transmissibility ratio	m	mass of the SDOF system
$G_{xx}(f, t)$	input time-varying nonstationary PSD	c	damping constant of the SDOF system
$G_{yy}(f, t)$	output response PSD by	k	Stiffness of the SDOF system
G_{rms_i}	GRMS value for i^{th} PSD position	T_f	Transfer function
f_u	Upper-frequency limit	c_{cr}	Critical damping of the SDOF
f_l	Lower frequency limit	β	Frequency ratio
$G_{rms_{i,j}}$	GRMS value for i^{th} PSD position j^{th} PSD segment	ζ	Damping ratio
P_k	Rayleigh probability for k th sigma stress region	m_i	The i^{th} spectral moment
E_{μ_k}	The k -th centroid position of Rayleigh distribution	d_i	Damage fraction
μ_k	The expected stress level for k th sigma stress region	v_p	Expected peak frequency number
S_{1g}	1G stress	v_0	Expected positive zero-crossing number
$S_{i,j}$	Applied stress under the j^{th} PSD segment in i^{th} PSD position	D	Cumulative damage
$N_{i,j}$	Life cycle time of the structure under the stimulation of j^{th} PSD segment in i^{th} PSD position	N	Life cycle time
D	Cumulative damage	n	Cumulative cycle time
f_n	The natural frequency of the structure	$E(D)$	Expected damage
$T_{i,j}$	The excitation time duration for the j^{th} segment in i^{th} PSD position	T	Time duration
$E(D)$	Expected damage	C	Coefficient from the S-N curve
u	Number of PSD positions	b	Slope of the S-N curve
v	Number of PSD segments	α	Irregularity factor
x	Generic random variable	$p(S)$	Stress range of PDF function
\ddot{x}	Base acceleration of the SDOF	λ_{oi}	The zero-order spectral moment for the i -th band
y	Mass Displacement of the SDOF	f_j	a central frequency of a narrowband

1. Introduction

Many mechanical components experience vibrational random loads in service. Fatigue failure of a single component or part may lead to complete failure of the system or machinery; therefore, fatigue failure is the most common type of failure mode induced under random loads. Vibration test and fatigue damage estimation methods are widely adapted for the fatigue assessment of mechanical components/structures subjected to random loadings. These structures and components are increasingly used even more complex and critical environments such as ground and aerial vehicles. The components are subjected to random loading conditions that are both difficult to model and expensive to test using current fatigue assessment methods [1]. Therefore, improved modeling techniques for the evaluation of fatigue performance of structures operating under extreme working conditions are needed.

Field and laboratory tests have been increasingly used for verification of machine designs [2]. In spite of their widely use and popularity, vibration tests can be prohibitively expensive and time-consuming; such tests usually require mechanical structures and components to be tested in the field and laboratory to simulate real loadings conditions during service lifetime [3,4]. Some high-cycle-lifetime components, such as jet engine components, feature testing cycles that can extend to 10^{10} cycles and can result in months of vibration testing under normal service loading conditions in the field or in laboratory [1]. Accelerated fatigue tests have been developed to simulate service loadings of the structural components mainly used in the automotive and aerospace industries in order to reduce time and cost [5-9]. Accelerated tests utilizes amplified load levels of random vibrations to test components so that the test time can be compressed on the basis of equivalent fatigue damage concept [6-8]. The applied random loadings are amplified during accelerated tests so that test time can be shortened such a way that accelerated test induce equivalent fatigue damage in which the tested components would normally experience in services. A random Gaussian process that can be described as a power spectral density (PSD) are used to represents random loads in the frequency domain [5,10]. The PSD can characterize the spread of the mean square vibration loadings over a frequency range [10]. Over past decades, a number of frequency-domain based fatigue estimation methods have been proposed to provide fatigue life assessment of structures by relating the PSD response and fatigue damage on the basis of a cyclic distribution of stresses [11-14]. The most methods mainly address the stationary Gaussian process represented a single stationary PSD. The PSD can be classified into narrow-band and wideband processes

dependent on a frequency band width of a given PSD function. A probability density function (PDF) of stress distributions for narrowband and wideband PSD functions can be associated to Rayleigh and Dirlik's distribution [8] respectively.

The narrow-band process was initially presented by Miles [15]. On the other hand, Bendat [16] first proposed a narrowband approach to estimate fatigue damage based on probability density function of the stress distribution. Bendat [16] showed that the probability stress peaks can be given by the Rayleigh distribution for the Narrowband process. Lutes and Sarkani [14] presented that the single moment (m_0) of the PSD function can be used to estimate the fatigue damage for the Narrowband method. In the narrow-band process, it is assumed that every stress peak is coincident with a cycle so the amplitudes of cycles can be related to the Rayleigh-distribution. The expected fatigue damage in the Narrowband method can be expressed in Eq. (1).

$$E(D) = \frac{v_0 T}{c} \int_0^\infty S^b \left(\frac{S}{4m_0} \exp\left(-\frac{S^2}{8m_0}\right) \right) dS \quad (1)$$

Where v_0 is the zero-mean up-crossing rate, T is the time duration, C and b are parameters to determine the S-N curve based on Eq. (2) [8].

$$NS^b = C \quad (2)$$

The fatigue damage induced by the i-th divided band can be calculated in Eqs. (3) and (4).

$$E(D) = \left(\sum_i^n d_i^{\frac{2}{b}} \right)^{\frac{b}{2}} \quad (3)$$

Where

$$d_i = \frac{b}{c} \Gamma\left(1 + \frac{b}{2}\right) v_0 \lambda_{0i}^{\frac{b}{2}} \quad (4)$$

Where v_0 is the central frequency of the i-th band, and λ_{0i} is the zero-order spectral moment for the i-th band.

The narrowband approach was found to be too conservative when it was applied to the wideband process [17]. This is based on the assumption that every peak coincides with a cycle. However, it yields too many cycles for a wide band process. The narrowband approach will result in very conservative results for wideband process. Light and Wirsching [18] and Dover and Kam [19] proposed various correction factors to reduce this conservative prediction of the narrowband approach. These methods provided some improvements on the narrowband process, however it was found to provide conservative results for other applications.

Dirlik [17] realized that the Rayleigh distribution is not appropriate for the Wideband process and proposed an empirical solution for the probability density function of rainflow stress ranges on the basis of first four moments of the PSD. In the Dirlik method, the PSD function is used to determine the first four moments of the PSD and then these four moments are used to obtain probability density function (PDF) of stress ranges.

Then, fatigue life is obtained by a damage accumulation method, e.g. Palmgren–Miner’s rule [20–21]. The PDF of stress distributions in Eq. (5) can be derived directly from moments (m_0 , m_1 , m_2 , and m_4) of the PSD function.

$$p(S) = \frac{\frac{D_1}{Q}e^{-\frac{Z}{Q}} + \frac{D_2}{R^2}e^{-\frac{Z^2}{2}} + D_3Ze^{-\frac{Z^2}{2}}}{2\sqrt{m_0}} \quad (5)$$

Where

$$\gamma = \frac{m_2}{\sqrt{m_0 m_4}}$$

$$X_m = \left(\frac{m_1}{m_0}\right) \sqrt{\frac{m_2}{m_4}}$$

$$Z = \frac{S}{2\sqrt{m_0}}$$

$$D_1 = \frac{2(X_m - \gamma^2)}{1 + \gamma^2}$$

$$D_2 = 1 - \gamma - D_1 + \frac{D_1^2}{1 - R}$$

$$D_3 = 1 - D_1 - D_2$$

$$R = \frac{\gamma - X_m - D_1^2}{1 - \gamma - D_1 + D_1^2}$$

$$Q = \frac{5(\gamma - D_1 - D_2 R)}{4D_1}$$

As can be seen from the equations above X_m , D_1 , D_2 , D_3 , Q and R are all functions of m_0 (zero-order moment), m_1 , m_2 , and m_4 .

The closed-form damage expression of the Dirlik method is defined as Eq. (6) below:

$$E(D) = \sum_i \frac{n_i}{N_i} = \sum_i \frac{p(S_i) v_p T dS}{N_i} \quad (6)$$

Where T is the time duration, v_p is the expected peak occurrence frequency number, and the stress range PDF function $p(S)$, is determined by Eq. (5).

Gao and Moan [22] recently proposed a trimodal method for a general wide-band process by splitting the power spectral density into three parts with equal variance. The authors used Hermite integration estimate the distribution of the sum of the multiple Rayleigh random variables. Zhao and Baker [23] formulated an expression for the cycle distribution on the basis of a linear combination of the Weibull and Rayleigh probability density function. Benasciutti and Tovo [24-25] proposed a frequency domain-method of fatigue damage estimation based on a linear combination of the upper and lower fatigue-damage intensity limits. Braccési et al. [26] proposed a damage estimation criterion called the bands method. The basic assumption of the bands method is that a given PSD function relevant to stress amplitude with both a narrowband and wideband can be divided into several bands. If the divided bandwidth can be summarized as the Rayleigh distribution of stress range, fatigue damage can be calculated by summing-up damages for each narrowband on the basis of Palmgren–Miner’s linear damage rule.

Despite considerable effort, most of frequency domain damage estimation methods are limited to stationary PSD function. However, many mechanical systems, such as tracked vehicles in real

service environments, cannot be accurately represented by a stationary random process [27]. Analysis and simulation of real loading conditions of those systems need to account for complex random loads in order to yield accurate damage predictions. For example, the tracked vehicle operational environment experiences complex random vibrational loadings that is a broadband random background with a strong influence of higher energy narrowband random vibration resulted from the interaction of the track with the terrain, roadwheels, and the vehicle drive sprockets. A swept frequency narrowband random vibration on wideband random vibration can best represent the realistic complex environmental loadings [27].

Fatigue damage predictions methods that account for complex random loads, provide more accurate results. Current fatigue damage predictions methods do not accurately consider the eventuality of a moving kurtosis matching the resonance frequencies. Therefore, an innovative damage modeling approach is proposed to compute fatigue damage in order to take into account non-stationary complex random loadings. A new modeling approach in the formulation of the novel numerical algorithm provides more accurate fatigue life assessment of engineering structural components by accurately accounting for complex random-on-random loadings (non-stationary PSD loadings) in comparison to stationary PSD based existing damage methods [14-19, 22]. The underlying concept of the proposed approach is based on a novel modeling framework that the time-varying non-stationary PSD function can be decomposed into a finite number of discrete stationary PSD functions. Each discrete PSD function represents the excitation energy level for a certain time span and can be further divided into a finite number of narrowband PSD segments. The fatigue damage is computed by summing up the damages associated with each narrow band according to the damage accumulation rule. Fatigue damage index is determined by accumulating damages of all discrete PSD positions. A numerical finite element (FE) method and experiments was used to simulate both PSD responses and the fatigue damage of three simplified aluminum structures which were designed to validate the proposed model. The proposed modeling capability to give more accurate fatigue life assessment of engineering structural components under complex random-on-random spectrum will provide a great advantage over experiments due to its simplicity, computational efficiency, and low cost.

2. Computational Modeling Approach

The proposed modeling approach is based on the key assumption that time-varying response PSD function can be transformed into discrete PSDs and each discrete PSD can be split into narrow

frequency bands so that stress spectrum can be determined in the form of a probability density distribution of a Rayleigh distribution. The Rayleigh distribution of stresses is subsequently used for the determination of cumulative fatigue damage through summation of damages for all discrete PSDs. A schematic representation of the computational modeling algorithm is shown Fig. 1. The computational modeling algorithm shown in Fig. 1, is proposed to implement fatigue damage assessments of the structural components that are subjected to time-varying complex spectrum loading conditions. Time-varying PSD function is obtained from the B1 tracked vehicle test spectrum of AECTP 400 standard describing a wideband random vibration superimposed by three sweeping high-amplitude narrowband [27].

The evolutionary response PSD for a structure can be computed from time-varying input PSD function by the transfer function of the structural dynamics. Time-varying PSD function can be considered as a generalization of discrete PSDs. More specifically, a time varying input PSD function can be decomposed into u number of finite input PSD positions and corresponding response PSDs can be computed using a transfer function of a given structure for all PSD positions. According to the bands method [26], each response PSD position is later divided into v number of narrow bandwidth segments; These segments are sufficiently narrow to assume that the process is narrowband one. Therefore, the stress distribution of each narrowband PSD segment can be characterized by the probability density function of a Rayleigh distribution. The fatigue damage for each response narrowband segment can be calculated by the stress-life curve (S-N curve). Finally, the cumulative fatigue damage for each PSD position can be determined by summing up damage values of each narrowband segment. In order to calculate the Fatigue Damage Index (FDI) for all PSD positions, the described modeling procedure is repeated for each PSD position of the full evolutionary PSD response function.

(Please refer to Fig. 1)

2.1. Input Power Spectrum Density

Many machine systems in service environments can experience complex random loadings due to operational requirements and service vibration conditions. Several standards such as MIL-STD 810 and AECTP 400, were developed to simulate actual operational vibrational loading conditions experienced by machine systems such as helicopters, tracked vehicles, and jet engines [27]. The AECTP 400 mechanical environmental tests are derived from field data representative of many

different vehicle types. A subset of AECTP 400 standard, the B1 tracked vehicle test spectrum, describes a wideband background random vibration superimposed by three sweeping high-amplitude random narrowbands [27], e.g. tracked vehicles such as tanks or a truck changing speed while driving over a rough road. The B1 test spectrum is selected as a representative time-varying input PSD function. This test spectrum is used in the proposed modeling approach in this paper because it accurately represents the complex vibration environment that is experienced by tracked vehicles. The B1 spectrum consists of three swept narrowbands and one stationary wideband random PSD. The first narrowband sweeps from 20 Hz to 170 Hz, the second one sweeps from 40 Hz to 340 Hz, and the third one sweeps from 60 Hz to 510 Hz. The sweep rate is defined within the range of one-half to one octave per minute. Table 1 shows the simplified sweep rates that are assumed to reduce the computational intensity of the model. According to Table 1, the simplified sweep rates for the first, second, and third narrowband are assumed to be 1 Hz/sec, 2 Hz/sec, and 3 Hz/sec, respectively.

A single sweep cycle includes one sweep up from the lowest sweep range to the highest sweep range, then followed by one sweep back down. As a result, each sweep from the lowest to highest frequency range takes 145 seconds on the basis of predefined sweep rates; Therefore, for computational simplicity, it is assumed that the complete PSD function including swept narrowbands are decomposed into 145 (u) independent discrete PSD positions. The input time-varying non-stationary PSD is denoted as $G_{xx}(f, t)$, so the relationship between the input PSD function and the discrete PSD positions can be expressed by Eq. (7).

$$G_{xx}(f, t) = \sum_{i=1}^n G_{xx_i}(f) \quad (7)$$

Where $G_{xx_i}(f)$ is the function of the discrete PSD position and n is equal to 1, 2, ..., u which represents the number of the PSD positions.

(Please refer to Table 1)

The PSD data presented in Table 1 are used to generate the wideband and swept narrowbands. Therefore, the PSD data in Table 1 are used as an input PSD function of the base excitation in the proposed modeling method. Figure 2 shows a schematic representation of time-varying input PSD function as a function of the frequency and time.

(Please refer to Fig. 2)

2.2. Modeling of Response PSD

Mechanical structures are usually subjected to an acceleration loading profile. A simple structural component shown in Fig. 3(a) that is subjected to random vibration loadings can be represented as a single-degree-of-freedom (SDOF) system in Fig. 3(b) provided that the first mode shape is dominant in the dynamic response of the structure. The modeling framework can be significantly simplified on the basis of the assumption of the SDOF [28-29]. The system equation of a damped SDOF is the equation of the base-excited function shown in Eq. (8):

$$m\ddot{y} + c(\dot{y} - \dot{x}) + k(y - x) = 0 \quad (8)$$

Where m is the mass of the system, and c and k are the damping and stiffness of the SDOF system, respectively.

(Please refer to Fig. 3)

The transfer function for a single-degree-of-freedom system is defined in Eq. (9). The transfer function which is the fundamental structural dynamic characteristics of the system can be used to relate input PSD to the response PSD.

$$T_f = \left| \frac{y}{x} \right| = \sqrt{\frac{1+(2\zeta\beta)^2}{(1-\beta^2)^2+(2\zeta\beta)^2}} \quad (9)$$

Where damping ratio $\zeta = \frac{c}{c_{cr}}$, critical damping $c_{cr} = 2mf_n$, natural frequency $f_n^2 = k/m$ and frequency ratio $\beta = f/f_n$. Eq. (9) shows that how the transfer function of the SDOF system can be related to the dynamic characteristics of the system in terms of a natural frequency and structural damping (e.t. damping mass, damping and stiffness of the system).

The relationship between the input PSD and response PSD of the given SDOF system can be expressed by the transfer function in Eq. (9). The input acceleration loading is denoted as the power spectrum density, $G_{xx}(f, t)$, and the output acceleration response PSD by $G_{yy}(f, t)$, the relationship between $G_{xx}(f, t)$ and $G_{yy}(f, t)$ is defined by Eq. (10) [14].

$$G_{yy}(f, t) = T_f^2 G_{xx}(f, t) \quad (10)$$

Similar to the input PSD, the continuous time-varying response PSD can also be decomposed into u number of discrete PSD positions. The discrete response PSDs can be expressed in Eq. (11).

$$G_{yy_i}(f) = \frac{1+(2\zeta\beta)^2}{(1-\beta^2)^2+(2\zeta\beta)^2} G_{xx_i}(f) \quad (11)$$

Where $G_{yy_i}(f)$ is the i -th number of the response PSD and $i = 1 \dots u$ (a number of PSD positions).

Figure 4 shows a response PSD obtained from a given input PSD on the basis of a SDOF system.

(Please refer to Fig. 4)

The input acceleration PSD can be also defined as the mean square amplitude of the acceleration with respect to the frequency. Unlike the phase information, all the amplitude information for the process is conserved in the PSD function. The root mean square (RMS) acceleration can be employed to quantify important statistical characteristics of the PSD function. The RMS acceleration is the square root of the area under the PSD function for a given frequency band. The root mean square acceleration is depicted as G_{rms} on the basis of the assumption that the gravitational acceleration (g) is considered as a unit. The value of G_{rms} can also represent average acceleration amplitude of the excitation in time domain. Based on the Wiener–Khinchine theory, G_{rms} for each response PSD position can be calculated by Eq. (12).

$$G_{rms_i} = \sqrt{\int_{f_l}^{f_u} G_{yy_i}(f) df} \quad (12)$$

Where, f_u and f_l are the upper and lower frequency limits of $G_{yy_i}(f)$ which is known as response PSD position, respectively.

The original input PSD function consists of the wideband with the range of 5 Hz to 2000 Hz and three narrowband that have been swept within the wideband range as described in Table 1. Each response PSD position $G_{yy_i}(f)$ can be further divided into a finite number of narrow frequency bands of the PSD segment. Each segment represents a narrowband PSD $G_j(f)$ with the central frequency located at f_j . The PSD division thus transforms a given discrete PSD, $G(f)$ into a finite set of narrowband PSD segments, $G_j(f)$, where $j = 1, 2, \dots, v$ [26]. To simplify the computational model and reduce computational intensity, each PSD position is split into a narrow frequency band of 1 Hz. Therefore, for each and every one of the u PSD decompositions described by Eq. (11) can be further divided into the v number of PSD narrowband segments with a frequency band of 1 Hz as depicted in Fig. 5.

(Please refer to Fig. 5)

2.3. Rayleigh Probability Distribution of Stresses

This section describes a method for derivation of cyclic stress distribution from the discrete response PSD. If each discrete response PSD function is divided into ν number of narrowband PSD segments, and each of narrowband PSD segments is associated with a different Rayleigh distribution of stress cycles. Each j -th narrowband segment characterized by a central frequency f_j where j is the number of the narrowband PSD segment, induces a different cycle as a function of f_j . The Rayleigh distribution can thus be used to describe the median and instantaneous peak of stresses, which in the current case represent the PSD narrowband. Each of the ν narrowband PSD segments can thus be represented by a different Rayleigh distribution that describes both the stress amplitudes and probability of the stress cycles as depicted in Fig. 6.

(Please refer to Fig. 6)

The Rayleigh distribution is expressed in Eq. (13).

$$f(x) = \frac{x}{\sigma^2} \exp\left(\frac{-x^2}{2\sigma^2}\right) \quad (x \geq 0) \quad (13)$$

Where, $f(x)$ is PDF of Rayleigh distribution.

To reduce the computational intensity of the modeling approach, the Rayleigh function describing each narrowband PSD segment is discretized. The random variable x used in the Rayleigh distribution is divided into five discrete stresses ($S_1 \dots S_5$) represented by $k = 1, 2, \dots, 5$ as shown in Fig. 7, and the probability distribution, P_k for each stress is calculated by Eq. (14) and results are given in Table 2.

$$P_k = \int_{(k-1)S}^{kS} x f(x) dx \quad (14)$$

Where, the k is stress region. It should be mentioned that k is equal to 1 to 5. Within the k th stress region, the lower stress value is $(k-1)S$, and the higher sigma value is kS .

(Please refer to Fig. 7)

To compute the stresses applied to the structure, the centroid position of the Rayleigh distribution is utilized. The centroid position divides each stress region into two parts of equal area and

represents the expectation value within each stress region. The centroid position μ_k is calculated by Eq. (15) and stress results are given in Table 2.

(Please refer to Table 2)

$$E_{\mu_k} = \int_{(k-1)S}^{\mu_k} xf(x)dx = \int_{\mu_k}^{kS} xf(x)dx \quad (15)$$

Where, E_{μ_k} represents the expected stress level at centroid point μ_k . The applied cyclic stresses associated with the Rayleigh distribution can be separated into k distinct stress amplitudes. S_k represent the expectation of the applied stress amplitude for each stress region. Therefore, the applied stresses corresponding to each narrowband PSD segment is calculated by Eq. (16).

$$S_k = S_{1g} \cdot G_{rms} \cdot E_{\mu_k} \quad (16)$$

Where S_{1g} is the 1G stress of the structure, G_{rms} is the area under the narrowband PSD segment, and E_{μ_k} is the expected stress level at centroid point μ_k .

For each PDF, the number of cycles, n_k , for applied stress, S_k , can be calculated in Eq. (17). Figure 8 shows the procedure that is needed to calculate results for n_k .

$$n_k = fTP_k \quad (17)$$

Where f is the response frequency, T is the time duration, and P_k the probability for each stress region of a given Rayleigh distribution.

(Please refer to Fig. 8)

2.4. Fatigue Damage

From the knowledge of applied stress ranges and cycles, the fatigue damage can be calculated by using the fatigue strength curve of the material i.e. S-N curve [30-34]. In order to compute fatigue damage for each of the ν PSD segments, the G_{rms} value is determined by Eq. (12). Then, k number of different applied stresses and corresponding stress cycles were calculated for each PSD segment by discretizing the Rayleigh distribution into k number of regions. A number of cycles, n_k and applied stresses, S_k , provides the information necessary to compute the fatigue damages for each

narrowband PSD segment; the number of cycles to failure, N for each narrowband PSD segment can be calculated from the traditional S-N curve in Eq. (18) and (19) as shown in Figure 7.

$$N_{j,k} = CS_{j,k}^{-b} \quad (18)$$

$$N_{j,k} = C \left(S_{1g} \cdot G_{rmsj} \cdot E_{\mu_{j,k}} \right)^{-b} \quad (19)$$

Where N is the number of cycles to failure, S is the stress amplitude, b is the slope of the S-N curve, and C is a constant corresponding to the material constant. Additionally, $k = 1 \dots 5$ and $j = 1 \dots v$ (the number of PSD segments). The S-N curve constants for the 5052-H32 aluminum alloy is given in Table 3.

Different stress regions in the PDF of Rayleigh distribution have different probabilities, as indicated in Table 2. Applied cycle numbers for each of the v PSD segments can be obtained by Eq. (20).

$$n_{j,k} = f_j T_j P_{j,k} \quad (20)$$

Where f_j is the central frequency of j -th response PSD band, T the time duration, and $P_{j,k}$ represents the probability of the Rayleigh stress distributions for the v -th PSD segments.

According to Palmgren–Miner's cumulative rule, fatigue damage for all PSD segments can be calculated by summing up the fatigue damages of damages of respective stress cycles of Rayleigh distributions derived from each PSD segment as expressed in Eq. (21).

$$d = \sum_{j=1}^v \sum_{k=1}^5 \frac{n_{j,k}}{N_{j,k}} \quad (21)$$

Where, v is the number of the PSD segments. Additionally, d is considered as damage per a PSD position.

Since d is damage per a discrete PSD position, after considering u number of discrete PSD positions, $n_{i,j,k}$ and $N_{i,j,k}$ can be determined by introducing i index such that $i=1 \dots u$. Thus, total fatigue damage index for u PSD positions can be calculated on the basis of Palmgren–Miner's rule in Eq. (22). The total (fatigue damage index) FDI can be formulated as the summation of the

damages that can be induced by each of the v PSD segments and each of the u PSD positions. According to Palmgren–Miner’s rule, total fatigue damage i.e. FDI is calculated by Eq. (22).

$$D = \sum_{i=1}^u d_i = \sum_{i=1}^u \sum_{j=1}^v \sum_{k=1}^5 \frac{f_{i,j} T_i P_k}{C \left(S_{1g} \cdot G_{rms_{i,j}} \cdot E_{\mu_k} \right)^{-b}} \quad (22)$$

2.5. Finite Element Modeling

The fatigue damage model described here was implemented through numerical codes in MATLAB and validated by FEA analysis and experimental tests. Both computational model and the FE method analyzed fatigue damages for three simple brackets designed specifically to ease the computational calculation. Aluminum 5052-H32 was chosen as the bracket material for evaluating the accuracy of the computational model. Material properties of the 5052-H32 aluminum alloy are given in Table 3.

(Please refer to Table 3)

Fatigue properties for the 5052-H32 aluminum alloy was obtained from test data up to 10^6 cycles. However, slope values for S-N curve for aluminum alloys are generally considered to have three different slopes over cycle ranges up to fatigue limit. Therefore, the assumption of the single constant slope may have some impacts on predicted fatigue damage results. Experimental modal tests were also conducted to provide additional validation data to verify and complement the FE results. The testing brackets were designed in such a way that they could be conveniently mounted on a shaker and experimentally tested as indicated in Fig. 9. Consequently, the area in contact with the shaker table that is subjected to the PSD base excitations. This area also constrains the bracket such that it only moves in the vertical direction and all other movement and rotation is minimized.

(Please refer to Fig. 9)

Based on the modal analysis, the fundamental shape of the bracket remained the same, but the natural frequency of each bracket was altered by simply fastening certain masses on the top flat plane. Element mesh size for the FE model of the brackets provided in Table 4 was employed to perform the required modal analyses and to determine the natural frequencies of the brackets. In order to further reduce computational intensity, a shell element was used mesh the FE model of the bracket as shown in Fig. 9. The original bracket without any mounted mass was designed to

have a natural frequency of 112 Hz, while small blocks of 254g and 527g rendered two additional structures with respective natural frequencies of 60 Hz and 40 Hz in Table 5. Mass of blocks are modeled by assigning a different material density on the top surfaces area shown as a violet color in Fig. 9(c).

(Please refer to Table 4)

The FE modal analysis of the brackets were conducted to determine the inherent modal characteristic of the structure featured by the mode shapes and natural frequencies. The computed natural frequencies derived from the FE modal analysis are found to be 40.4Hz, 58.1Hz and 113.5Hz as listed in Table 5., these calculated natural frequencies are slightly different than intended values of 40Hz, 60Hz and 112z. The 1st mode of interest was determined to be a bending mode illustrated in displacement pattern in Fig. 10, and this modal result verifies the validity of the SDOF assumption.

(Please refer to Fig. 10)

Following modal analyses, a FE spectrum analysis was performed to simulate the structural dynamic response (the response PSD) of the three brackets subjected to the input PSD function. The spectrum analysis obtained by the ANSYS software package was able to perform one PSD analysis per run job. The time varying PSD function was decomposed into the number of independent PSDs. The number of independent PSDs was chosen to be equal the number of computational runs (discrete PSD positions in time) so that discrete input and response PSDs were consistent between the computational model and the FE model. Therefore, the time varying PSD was decomposed into 145 independent PSDs. The moving rate for the first narrowband was set to 1 Hz/sec and the moving rate for the second and the third narrowband were set to 2 Hz/sec and 3 Hz/sec, respectively. After performing each of the 145 computation runs, the lower frequency of each narrowband increases because of the moving rate. For instance, at the 20th computation run, the lower frequency of the first, the second, and the third narrowband increases from 20 Hz to 40 Hz, 40 Hz to 80 Hz, and 60 Hz to 120 Hz, respectively. On the other hand, the bandwidth of each narrowband remains constant throughout the entire swept range as per Table 1.

In order to compute the fatigue damage, calculating 1G stress for each three brackets is necessary. Because the Rayleigh distribution was used to represent the stress distribution, and this

distribution differs from the ANSYS default setting. The 1G stress for each bracket was obtained from the static linear analysis in ANSYS. Four fictional bolt holes were introduced to better simulate a scenario where the brackets would be tested on a shaker table, and the FE models were also constrained at those four points during the static analysis. The 1G stress results for all three brackets at the critical location shown in Fig. 11 are given in Table 5.

(Please refer to Fig. 11)

(Please refer to Table 5)

3. Discussion and Results

As a part of the validation process, the modal tests were conducted on test bracket samples using a random excitation sweep from 1-500Hz to identify a natural frequency of the bracket components generating peak response in the frequency response spectrum.

The computed natural frequencies obtained from the FE modal analysis agree well with the experimental frequencies obtained from the modal test as shown in Fig. 12. The FE modal results are compared with experimental frequencies in Table 6 and error values is found to be in range of approximately 4-7%.

(Please refer to Table 6)

(Please refer to Fig. 12)

The PSD spectrum tests were not conducted due to the lack of appropriate software package for the shaker controller to carry out the time-varying PSD excitations. The input acceleration PSD function consists of a wideband and three sweeping narrowbands. Because of the dynamic nature of these narrowbands, the resonance behavior of the structure is expected to change., the bracket undergoes through three distinct dynamic response behaviors. Three distinct sweeping narrowbands have the potential to induce significant fatigue damages when any of narrowbands matches with the natural frequency of the given brackets. Three different brackets were designed and analyzed in order to assess the impact of the different natural frequencies on the PSD response and fatigue damage the structural brackets.

Figure 13 presents a three-dimensional surface of the PSD response estimated by the computational model, as a function of the frequency and PSD position in time. Figure 13 shows that each bracket with a different natural frequency introduces a different PSD response. There are three ridges, and one hilly shaped surface of the PSD response. The three curving ridges are induced by the sweeping narrowbands, and the peak hilly shape PSD surface is resulted from the dynamic response characteristic of the structure (the natural frequency of the structure) due to the wideband PSD excitation. The response PSDs computed from the computational model shown in Fig. 13 provides good insight the effects of natural frequency of the brackets in the dynamic response. The ridges are arranged closely near lower natural frequency (e.g. 40 Hz) and increasingly become scattered for higher natural frequency (e.g. 112 Hz) The response PSD generated from both FEA and computational models were compared at five different discrete PSD positions as shown in Fig. 14.. Based on the PSD responses for three different brackets, PSD responses of the computation model are in good agreement with ones of the FEA method even though that the model slightly overestimates the PSD responses in higher and lower ends of frequency ranges for the three brackets.

(Please refer to Fig. 13)

(Please refer to Fig. 14)

The response PSD includes time-varying complex PSD function induced by the high-power sweeping narrowbands imposed on wideband PSD. Non-stationary PSD loadings result in a significantly greater fatigue damage in comparison to stationary PSD loadings [35-36]. Therefore, the Dirlik and narrow band damage methods [14-19] are not considered to be appropriate damage modeling methods for fatigue damage assessment of the structures subjected to this type of non-stationary PSD loadings. A novel computational modeling approach is developed to estimate fatigue damage of structural components subject to complex non-stationary random loadings. The fatigue damage for each of the Rayleigh distributions determined from individual narrowband segments was calculated based on Palmgren–Miner’s rule., the cumulative FDI can be obtained by summing up damages of each of all discrete PSD positions.

The FDI values of three different brackets are calculated from both the computational model and FEA method in Table 7. The prediction error values of FDI between the FEA method and computational model is listed in Table 7. The relatively small FDI values reported in Table 7 are

contributed to very low 1G stresses incurred by the test structure. Since the weight of the brackets designed in the scope of this paper were relatively very small, they were consequently subject to very low 1G stresses of around 2 MPa, i.e. very low PSD stresses. The FDI error calculated was less than 44% for the bracket with 40 Hz natural frequency, less than 28% for the bracket with 60 Hz natural frequency, and less than 5% for the bracket with 112 Hz natural frequency.

(Please refer to Table 7)

Figure 15 represents a 3D fatigue damage index surface (FDI) as a function of both the natural frequency and 1G stresses associated with any structure. A red surface illustrates the fatigue damage failure plane when the FDI is considered to be unity. Moreover, the blue surface represents the equivalent FDI values for various frequencies and 1G stresses of a given structure. The plane at which the FDI is equal to unity divides the FDI surface into two parts: The part below the red surface and the part above the red surface. Each point located on the lower part below the red plane indicates that under any combination of natural frequencies and 1G stresses, the structure will survive the four-hour AECTP 400 testing under the applied time varying PSD. By contrast, points located on the FDI surface the above the red plane indicate that the structure will fail before the four-hour testing is over.

(Please refer to Fig. 15)

The computational model was developed to optimize the design of structures subject to complex random vibration loadings. Since both FEA and computational models showed good correlation, a more general tool with capabilities extending to multiple degree of freedom systems can be potentially developed in the future. Furthermore, Complex structures can be considered multi-degree-of freedom systems and their dynamic characteristics can be easily determined by FEA. For selected geometrical locations and geometrical discontinuities on the structure, the response characteristics of displacements, stress and acceleration can be obtained through the appropriate frequency transfer function. Therefore, the proposed modeling approach can be integrated with commercial FE packages or fully implemented with finite element codes.

4. Conclusion

The proposed modeling approach work is innovative in its algorithm formulation to efficiently and accurately compute fatigue damage of simplified structural components under complex random-

on-random vibrational loadings in the form of accelerated time-dependent PSD function. Because of the novel possibility of PSD decomposition and narrowband division of PSD positions, a given non-stationary PSD function was decomposed into a finite number of the discrete PSD positions and each of these PSD positions was split into narrowband PSD segments in which the Rayleigh distribution of stresses could be associated to narrowband PSD segments. The fatigue damage estimation was obtained by adopting the stress-life and the cumulative damage method. The FE models of three bracket structures with different natural frequencies were used to obtain numerical FEA data to validate the computational model. The computational model results showed a good correlation with the FEA data for PSD responses and FDI values.

The computed PSD responses indicate that the swept narrowbands of the input PSD is of considerable significance in the fatigue damage of the structures subjected to the time-varying random PSD loadings. The 3D FDI surface shows that the fatigue damage increases rapidly as the 1G stress increases or the natural frequency goes up. Higher 1G stress leads to higher applied stresses under the same input PSD loadings, and a higher natural frequency means that more cycle times occur during resonance within the same time duration. The higher applied stress and increased cycle times under resonance will cause more fatigue damage to the structure and accelerate fatigue failure. Reducing the natural frequency of the structure, its interaction with the sweeping narrowbands and decreasing the applied stresses on the structure can reduce fatigue damage experienced by the structure. Moreover, designing the natural frequency of the structure to be away from the frequencies of the swept narrowband inputs can also contribute to extending lifetime.

The modeling approach presented here shows that a novel computational modeling technique can be employed to accurately simulate accelerated test conditions for simplified mechanical structures and components subjected to complex random vibrational excitations. The structural components could be modeled as an SDOF system provided that they would experience single dominant modes shape to participate in the dynamic response of the structure. This assumption was mainly made to simplify computational burden of the proposed modeling approach. However, the modeling approach appears to be quite promising due to its strong correlation with the FEA numerical data. The proposed approach can be extended to more complex structural components that can be represented as multiple degrees of freedom systems. The modeling framework developed here can be easily adapted to optimize the design of many structural components in the

early design phase prior to building prototypes for laboratory or field vibration tests. The proposed modeling approach provides significant advantages compared to accelerated vibrational tests and FEA in terms of the computational efficiency and cost.

References

1. Hoksbergen, J., Defining the Global Error of a Multi-Axis Vibration Test, *Sound and Vibration*, Vol. 48(9), pp.8-13, 2014.
2. Habtour, E., Connon, W.S., Pohland, M.F, Stanton, S.C., Paulus, M., and Dasgupta, A., Review of response and damage of linear and nonlinear systems under multiaxial vibration, *Shock and Vibration*, Article ID 294271, 21 pages, 2014.
3. Steinwolf, A., Shaker random testing with low kurtosis: Review of the methods and application for sigma limiting, *Shock and Vibration*, Vol.17(3), pp. 219-231, 2010.
4. Rotem, A., Accelerated fatigue testing method, *International Journal of Fatigue*, Vol.3(4), pp. 211-215, 1981.
5. Allegri, G. and Zhang, X., On the inverse power laws for accelerated random fatigue testing, *International Journal of Fatigue*, Vol.30(6), pp. 967-977, 2008.
6. Özsoy, S., Celik. M. and Kadioğlu, F.S., An accelerated life test approach for aerospace structural components, *Engineering failure analysis*, Vol.15(7), pp.946-957, 2008.
7. Shires, D., On the time compression (test acceleration) of broadband random vibration tests, *Packaging Technology and Science*, Vol.24(2), pp. 75-87, 2011.
8. Xu, K., Development of vibration loading profiles for accelerated durability tests of ground vehicles, PhD thesis, University of Manitoba, 2011.
9. Eldoğan, Y., and Cigeroglu, E., Vibration fatigue analysis of a cantilever beam using different fatigue theories, In *Topics in Modal Analysis*, Vol.7, pp.471-478, 2014.
10. Wolfsteiner, P., and Sedlmair, S., Deriving gaussian fatigue test spectra from measured non gaussian service spectra, *Procedia Engineering*, Vol.101, pp. 543-551, 2015.
11. Lutes, L.D., and Larsen, C.E., An improved spectral method for variable amplitude fatigue prediction, *J Struct Div., ASCE*, Vol.116, pp.1149–64, 1990.
12. Wirsching, P.H., Light, M.C., Fatigue under wide band random stresses, *J Struct Div., ASCE*, Vol. 106(ST7), pp.1593–607, 1980.

13. Braccresi, C., Cianetti, F., Lori, G., Pioli, D., Fatigue behaviour analysis of mechanical components subject to random bimodal stress process frequency domain approach, *Int J Fatigue*, Vol.27(4), pp.335–45, 2005.
14. Lutes, L.D., and Sarkani, S., *Random vibrations: analysis of structural and mechanical systems*, Butterworth-Heinemann, 2004.
15. Miles J.W., On structural fatigue under random loading, *J Aeronaut Soc.*, Vol.21, pp.753–62, 1965.
16. Bendat J., Probability functions for random responses. In: NASA report, 1964.
17. Dirlik, T., Application of computers in fatigue analysis, Doctoral dissertation, University of Warwick, 1985.
18. M. Light and P. Wirsching, Fatigue under wide band random loading, *J Struct*, pp. 1593-1607, 1980.
19. W. Dover, J. Kam, Fast fatigue assessment procedure for offshore structures under random stress history, *Proc. Instn. Civ. Engrs*, Vol. 2(85), pp. 689-700, 1988.
20. Palmgren A., Die lebensdauer von kugellagern, *VDI-Zeitschrift* Vol.68, pp.339–341, 1924.
21. Miner, M.A., Cumulative damage in fatigue, *J Appl Mech*, Vol.12, pp.159–64, 1945.
22. Ghao Z, Moan T., Frequency-domain fatigue analysis of wide-band stationary gaussian processes using a trimodal spectral formulation, *Int J Fatigue*, Vol.30(10–11), pp.1944–55, 2008.
23. Zhao W, Baker MJ, On the probability density function of rainflow stress range for stationary gaussian processes, *Int J Fatigue*, Vol.14(2), pp.121–35, 1992.
24. Tovo R., Cycle distribution and fatigue damage under broad-band random loading, *Int J Fatigue*, Vol.24(11), pp.1137–47, 2002.
25. Benasciutti, D., and Tovo, R., Fatigue life assessment in non-Gaussian random loadings, *International journal of fatigue*, 28(7), pp.733-746, 2006.
26. Braccresi, C., Cianetti, L., Tomassini., Random fatigue. A new frequency domain criterion for the damage evaluation of mechanical components, *International Journal of Fatigue*, Vol.70, pp.417-427, 2015.
27. NATO/PFP UNCLASSIFIED, "AECTP 400 (Edition 3) – MECHANICAL ENVIRONMENTAL TESTS", 2006
28. Gatti, P. L., *Applied Structural and Mechanical Vibrations: Theory and Methods*, CRC Press, 2014.

29. Crandall, S. H., and William D. M., Random vibration in mechanical systems, Academic Press, 2014.
30. Ince, A., A mean stress correction model for tensile and compressive mean stress fatigue loadings, *Fatigue and Fracture of Engineering Materials and Structures*, Vol. 40(6), pp. 939-948, 2017.
31. Ince, A., A generalized mean stress correction model based on distortional strain energy”, *International Journal of Fatigue*, Vol.104, pp.273-282, 2017.
32. Ince, A., A novel technique for multiaxial fatigue modelling of ground vehicle notched components, *International Journal of Vehicle Design*, Vol. 67, pp.294-313, 2015.
33. Ince, A., and Bang, D., Deviatoric Neuber method for stress and strain analysis at notches under multiaxial loadings, *International Journal of Fatigue*, Vol.102, pp.229-240, 2017.
34. Ince, A. and Glinka, G., A generalized damage parameter for multiaxial fatigue life prediction under proportional and non-proportional loadings, *International Journal of Fatigue*, Vol. 62, pp. 34–41, 2014, doi: 10.1016/j.ijfatigue.2013.10.007.
35. Capponi, L., Cesnik, M., Slavic, J., Cianetti, F., Boltezar, M., A mean stress correction model for tensile and compressive mean stress fatigue loadings, *International Journal of Fatigue*, Vol. 104, pp. 221-230, 2017.
36. Kihma, F., Fergusonb, N.S., Antonic, J., Fatigue life from kurtosis controlled excitations, *Procedia Engineerin*, Vol. 133 pp. 698 – 713, 2015.

List of Tables

Table 1. Heavy vehicle schedule breakpoints [27]

Table 2. Discretized stress regions of Rayleigh distribution

Table 3. Material Properties of Aluminum 5052-H32

Table 4. Mesh properties of FE model

Table 5. FE 1G static and modal analysis

Table 6. Natural frequency comparison between modal test and FE modal analysis

Table 7. FDI comparison between the model and FEA

List of Figures

Figure 1. Schematic representation of proposed fatigue damage modeling for time-varying PSD

Figure 2. Schematic representation of time-varying input PSD

Figure 3. Schematic representation of single-degree-of-freedom (SDOF) system

Figure 4. The process of producing a response PSD for a given PSD input by the given SDOF system

Figure 5. Schematic representation of division of a given PSD into number of narrowbands

Figure 6. A schematic representation of narrowband division and corresponding PDF of stress distribution

Figure 7. A schematic representation of discretized stress regions in Rayleigh distribution

Figure 8. Schematic representation of procedure to obtain N and n for a narrowband PSD segment

Figure 9. (a) Bracket configuration with added weight to obtain natural frequencies of 40,60 and 112 Hz; (b) a scheme of the mode shape of the first natural frequency of all three brackets

Figure 10. Modal shape of structural bracket

Figure 11. von Mises stress contour plot

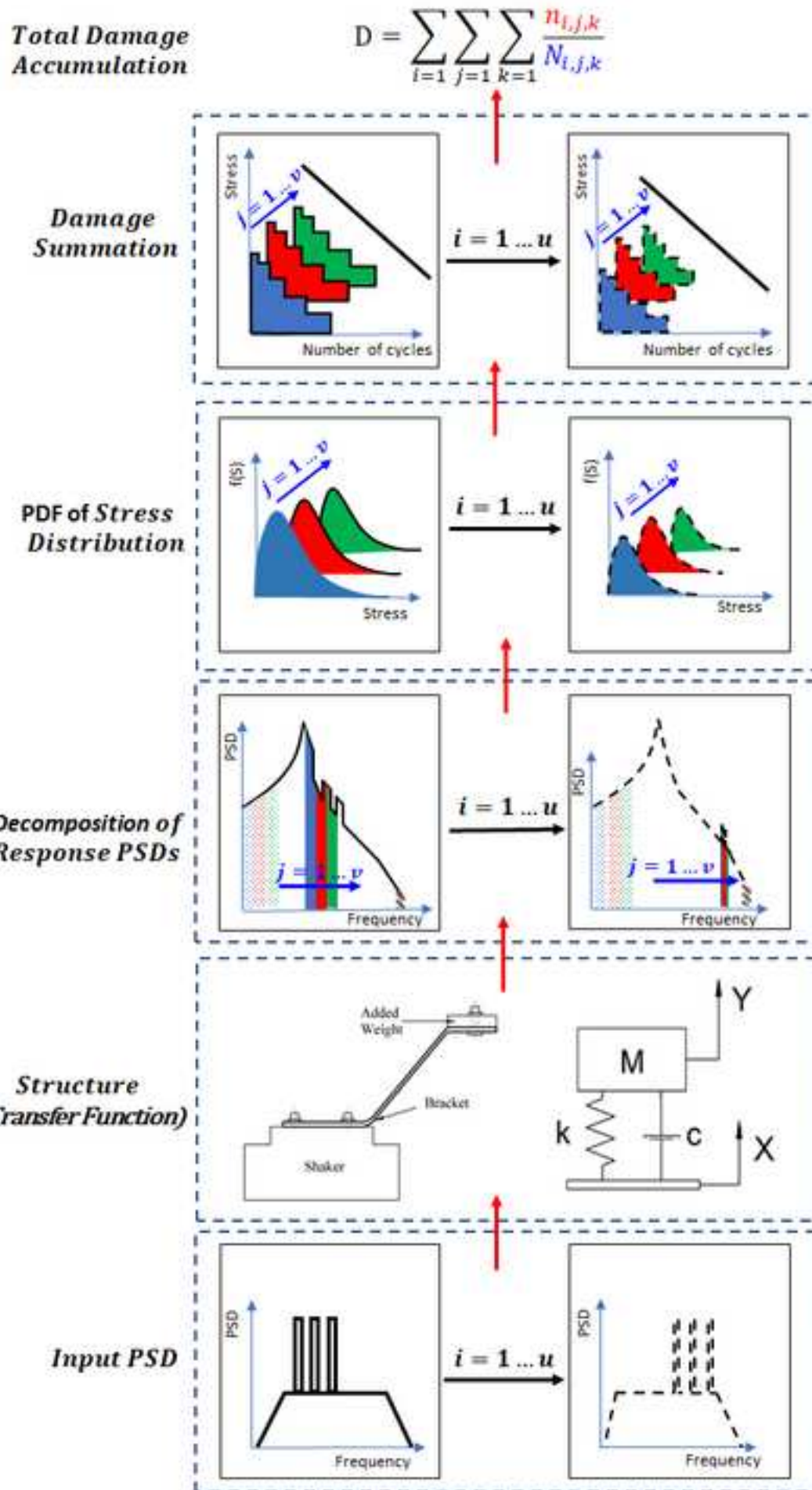
Figure 12. Natural frequency between modal test and FEA for a bracket of (a) 40 Hz natural frequency (b) 60 Hz natural frequency (c) 112 Hz natural frequency

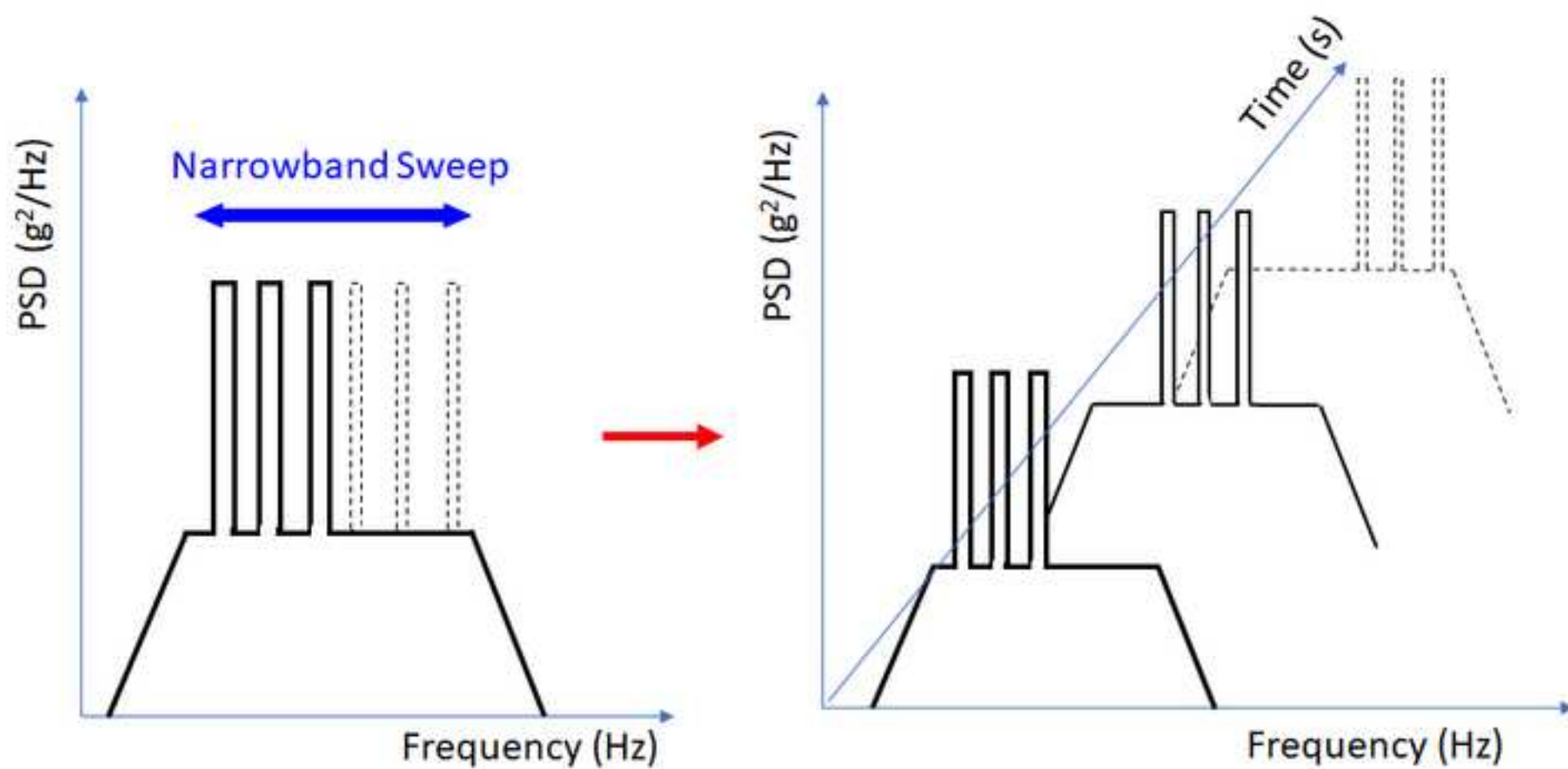
Figure 13. Response PSD of model for (a) 40 Hz bracket; (b) 60 Hz bracket; and (c) 112 Hz bracket

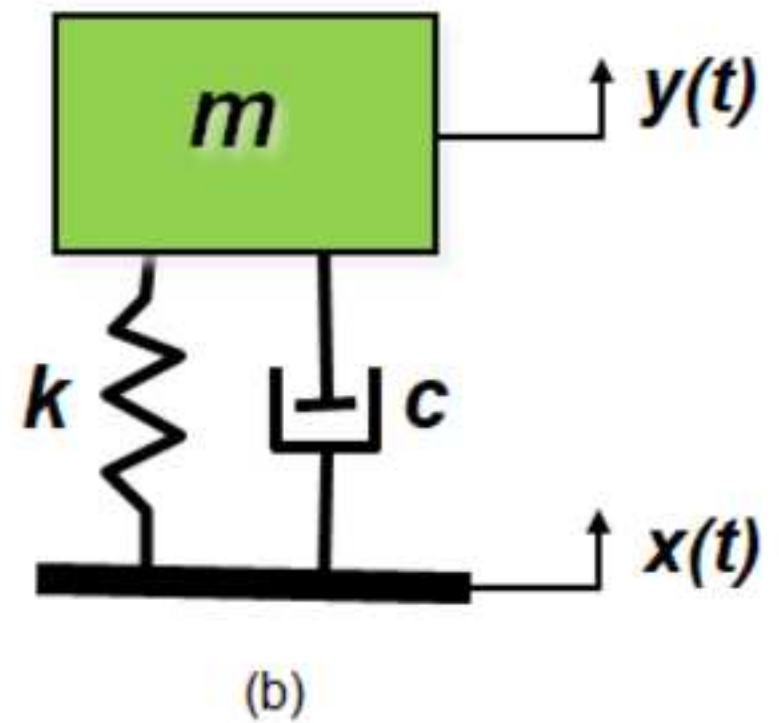
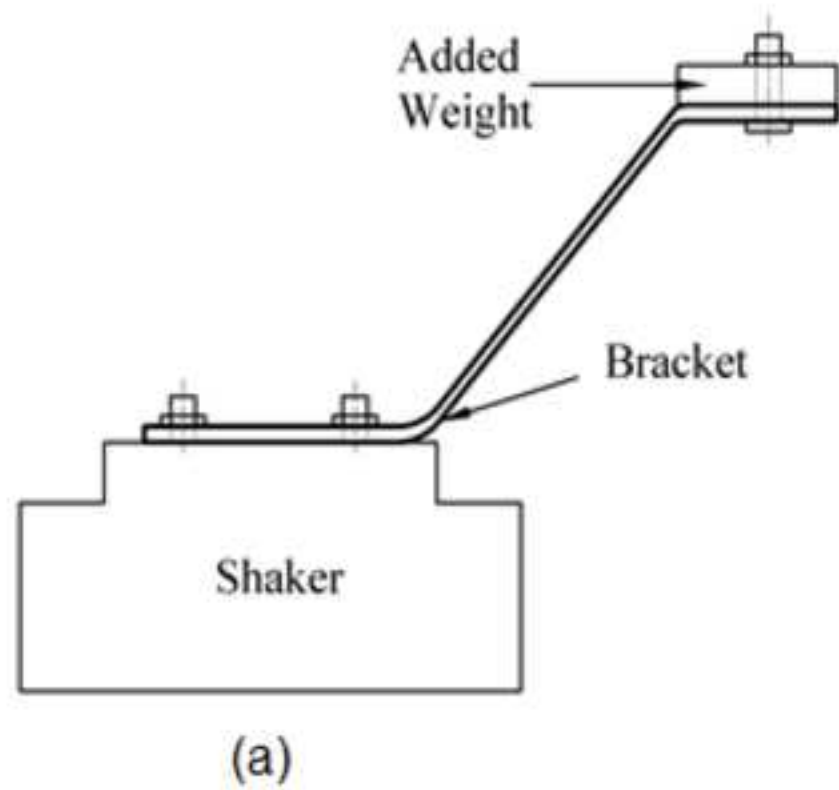
Figure 14. Response PSD comparison between the model and FEA for (a) 40 Hz bracket; (b) 60 Hz bracket; and (c) 112 Hz bracket

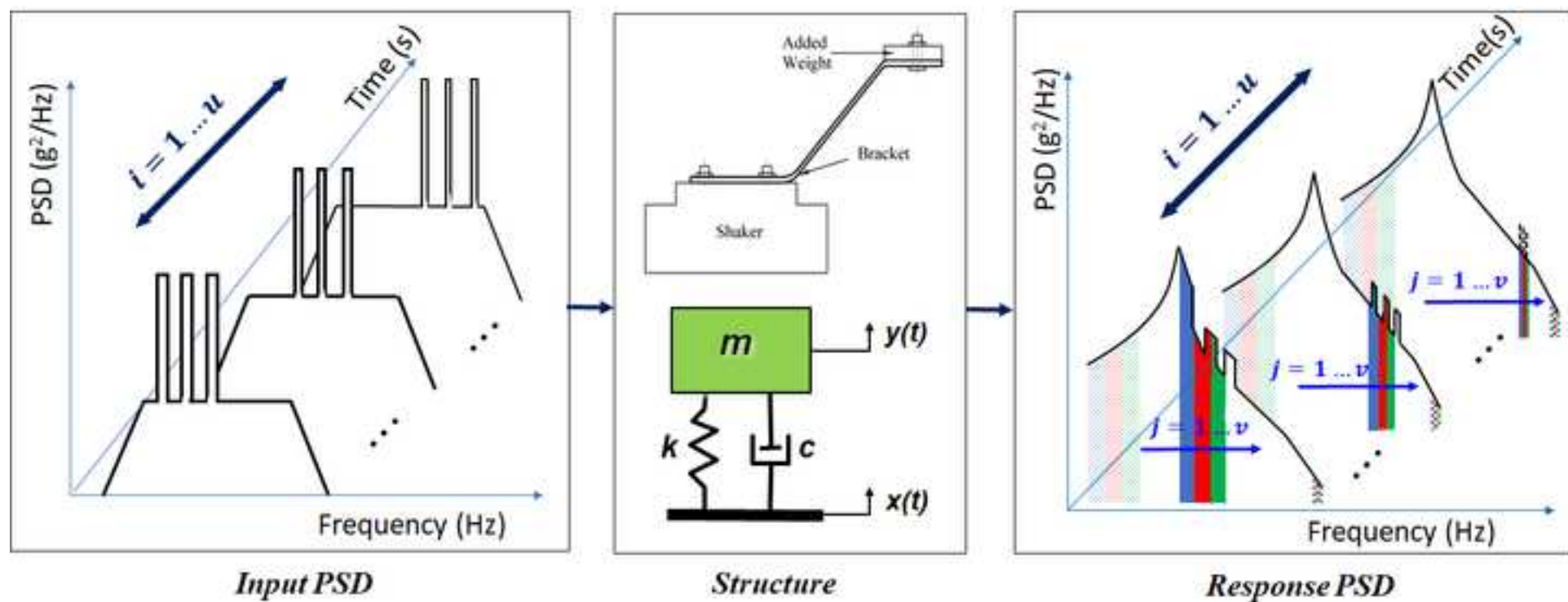
Figure 15. FDI values for different 1G stresses and natural frequencies

ACCEPTED MANUSCRIPT









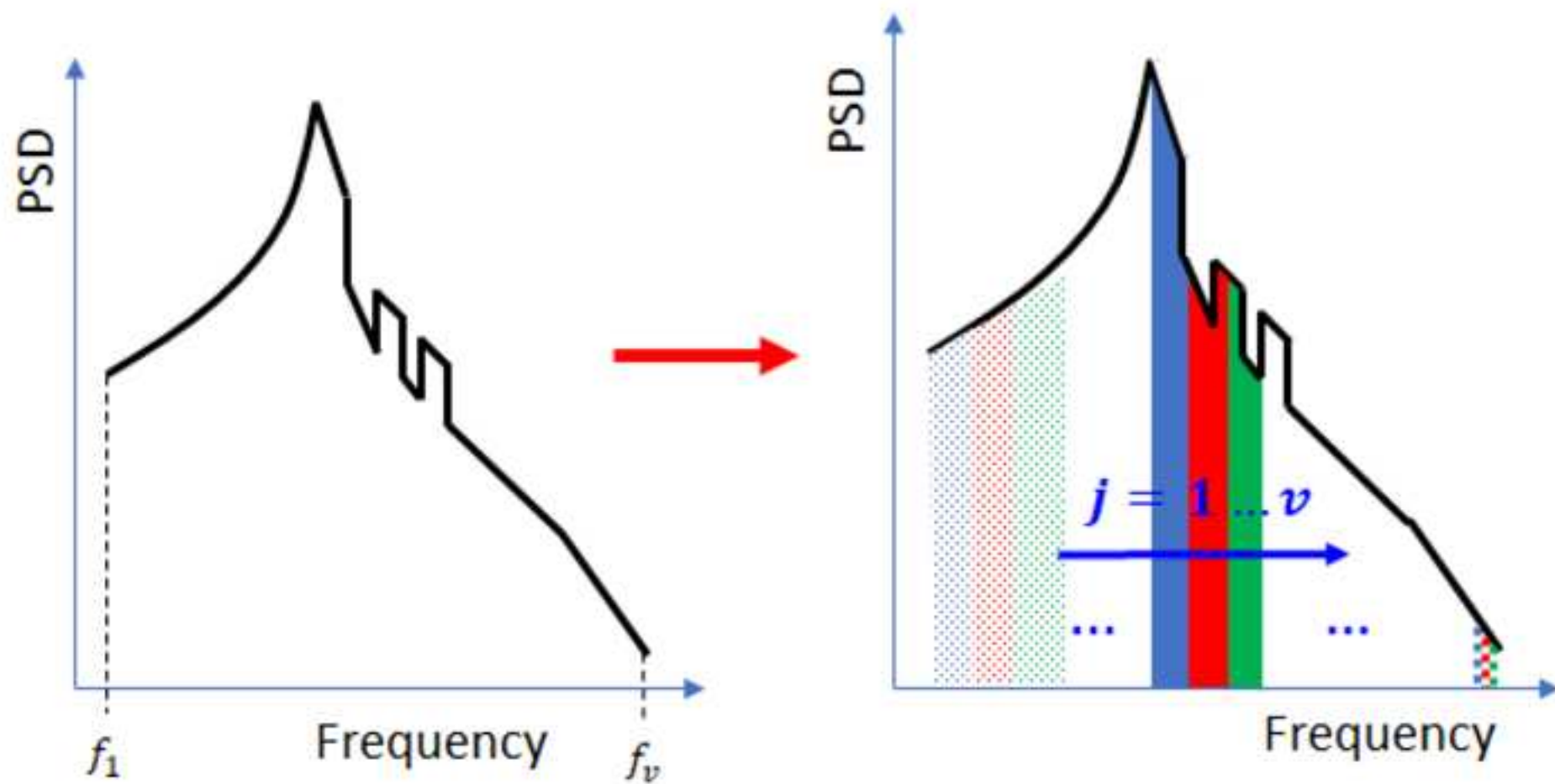
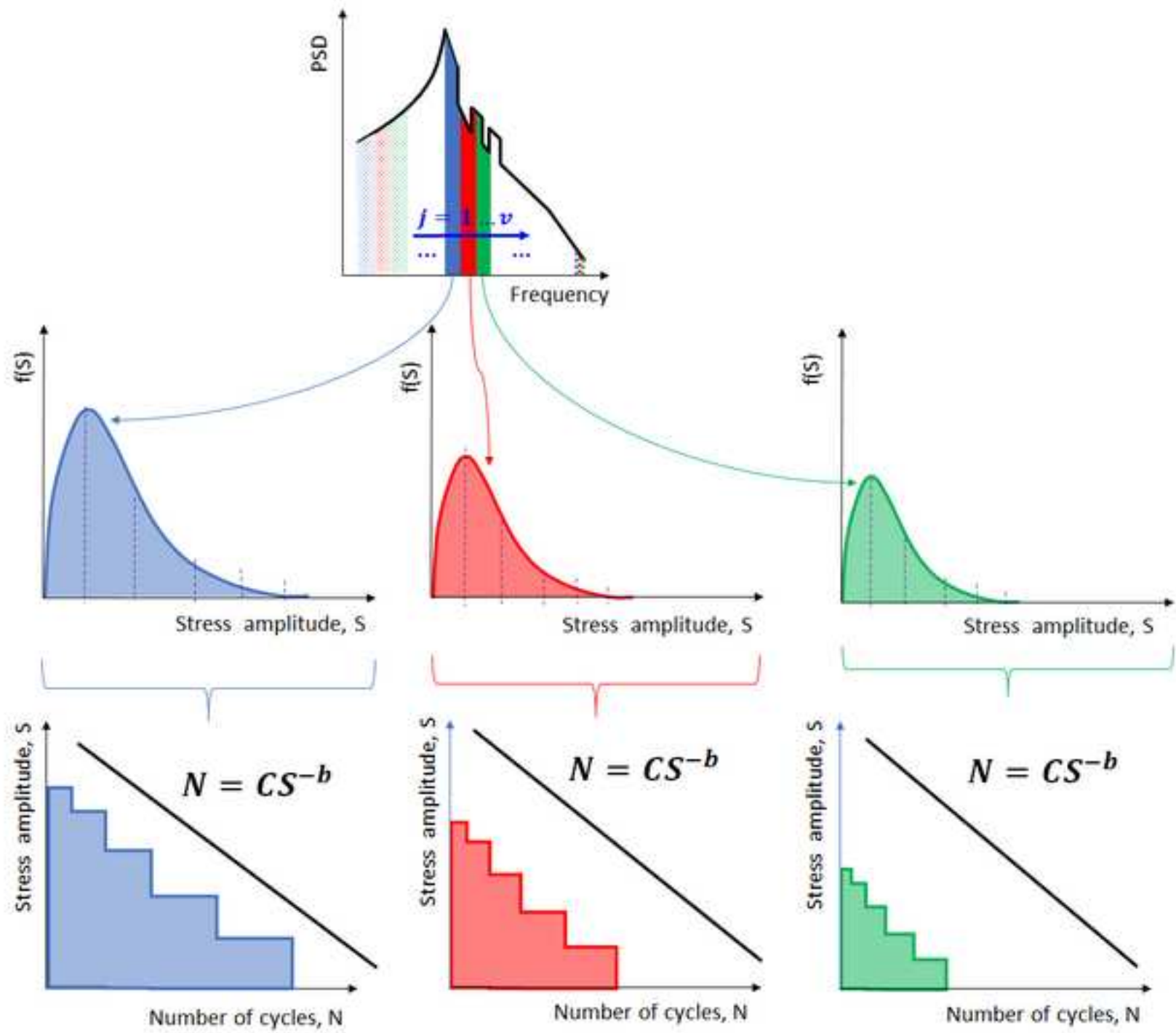
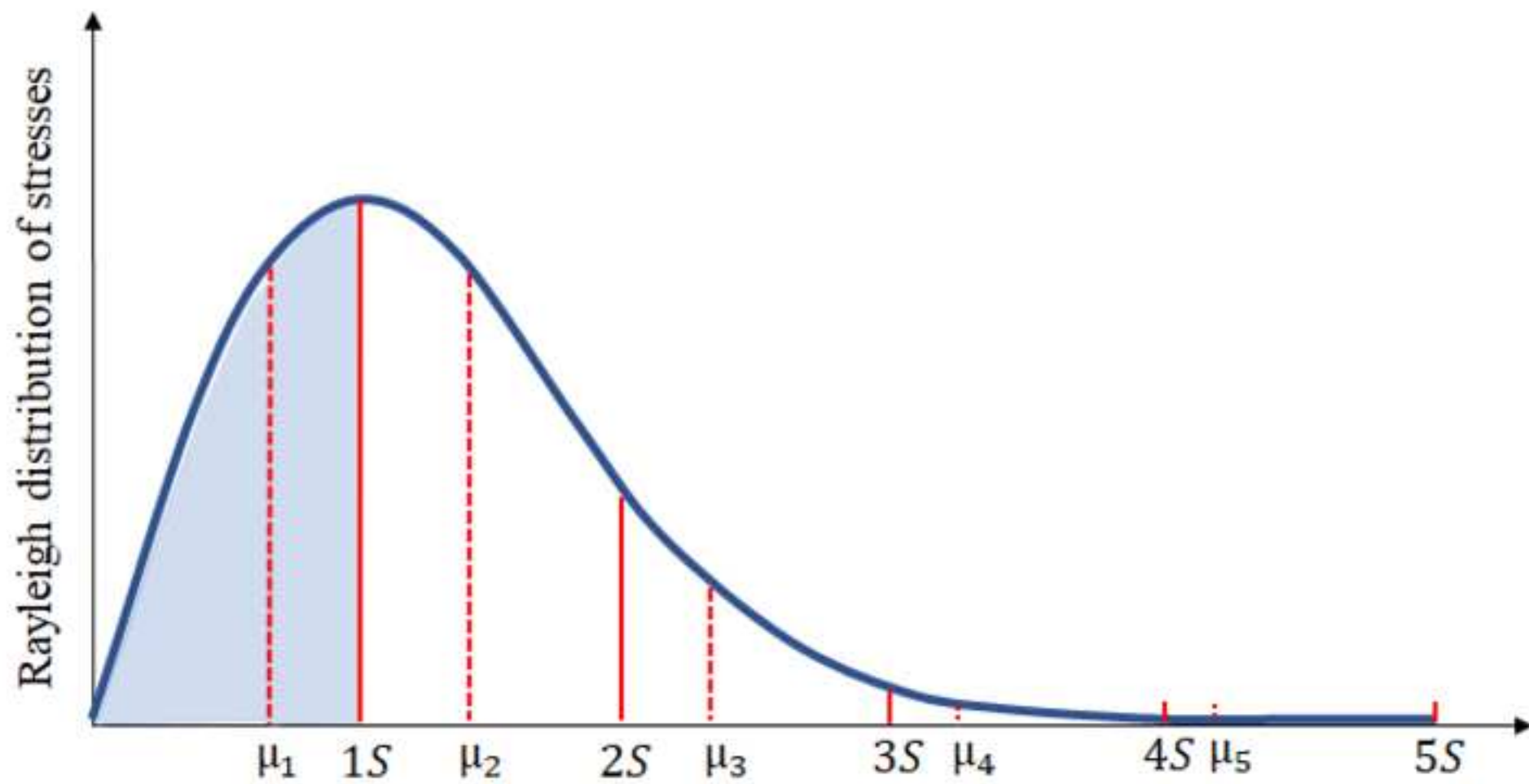
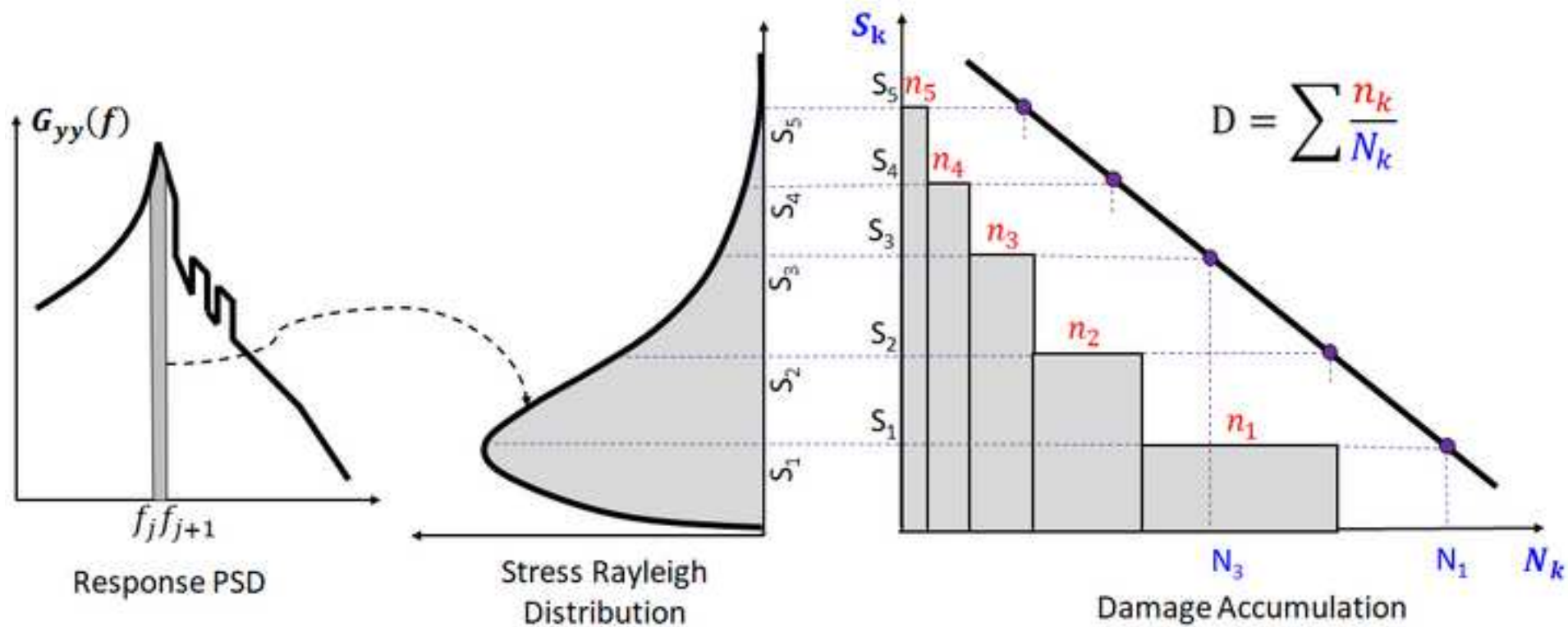
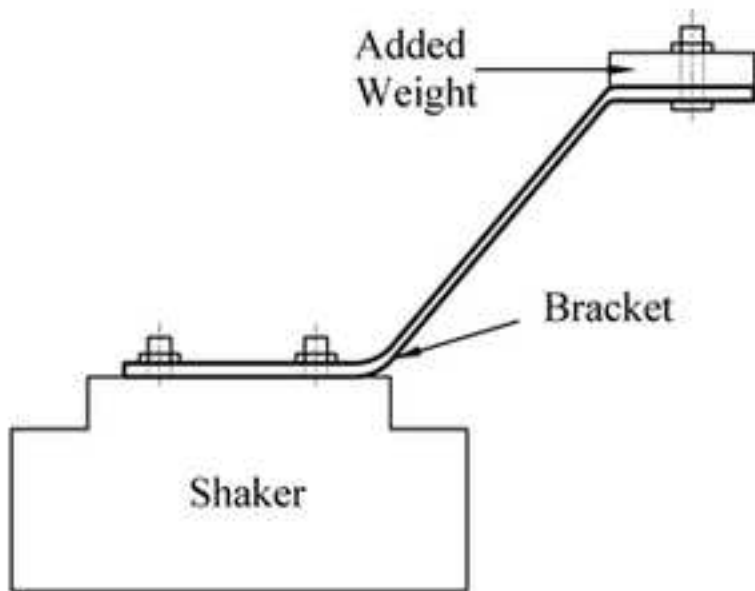


Figure 6

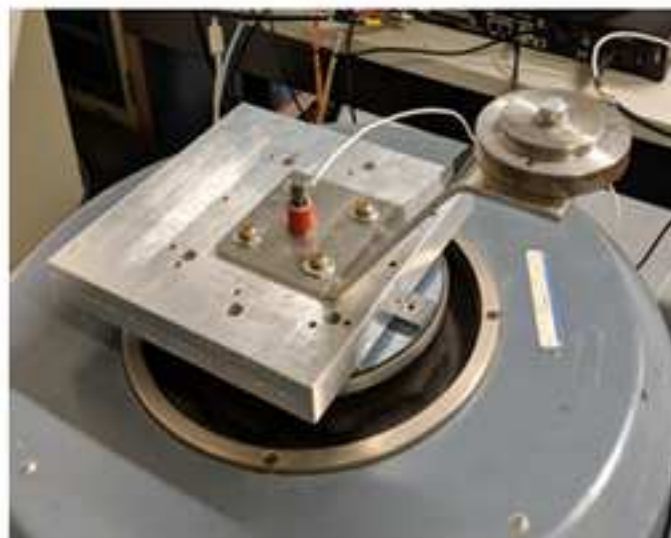








(a)



(b)



(c)

Figure 10

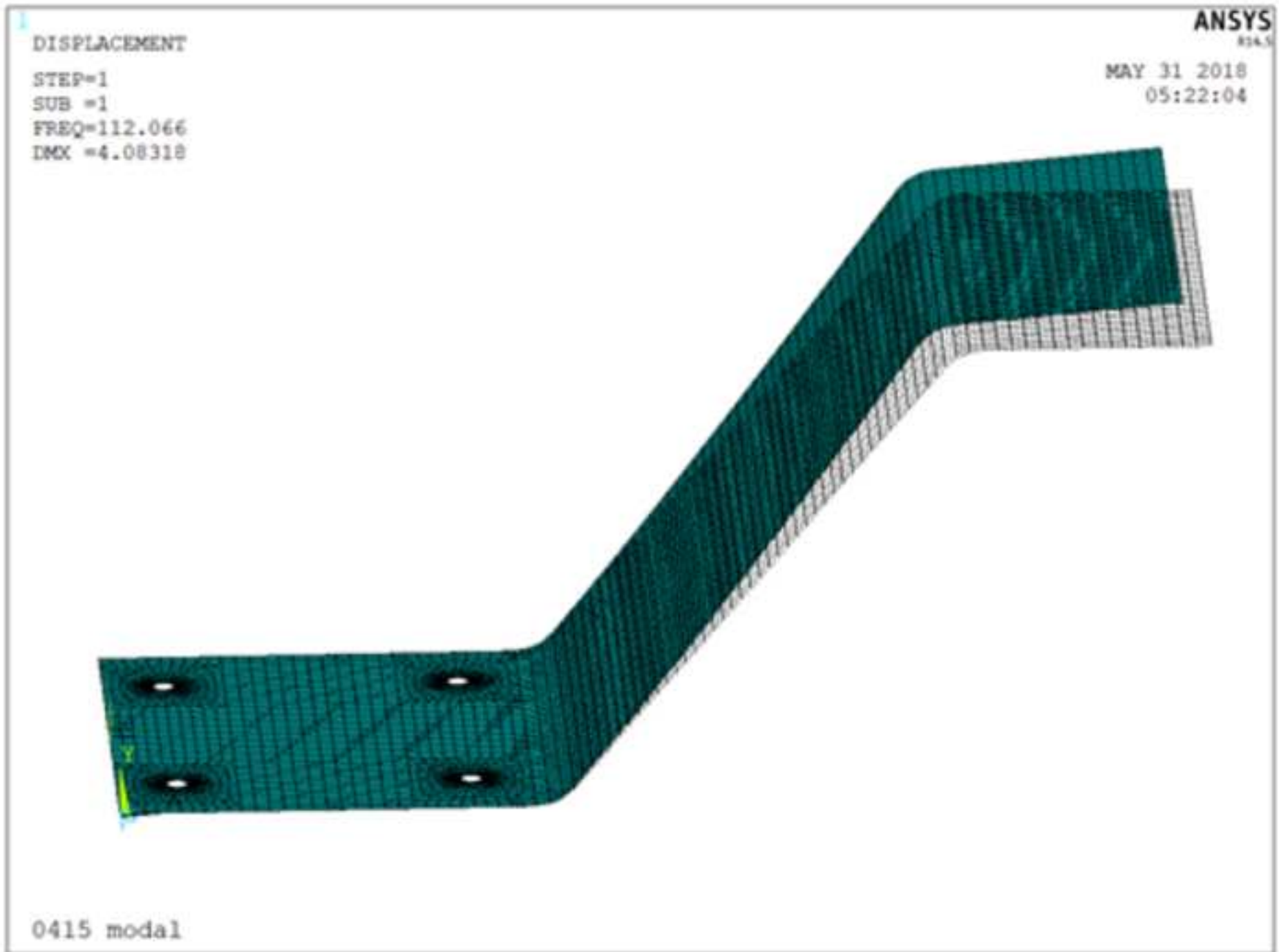
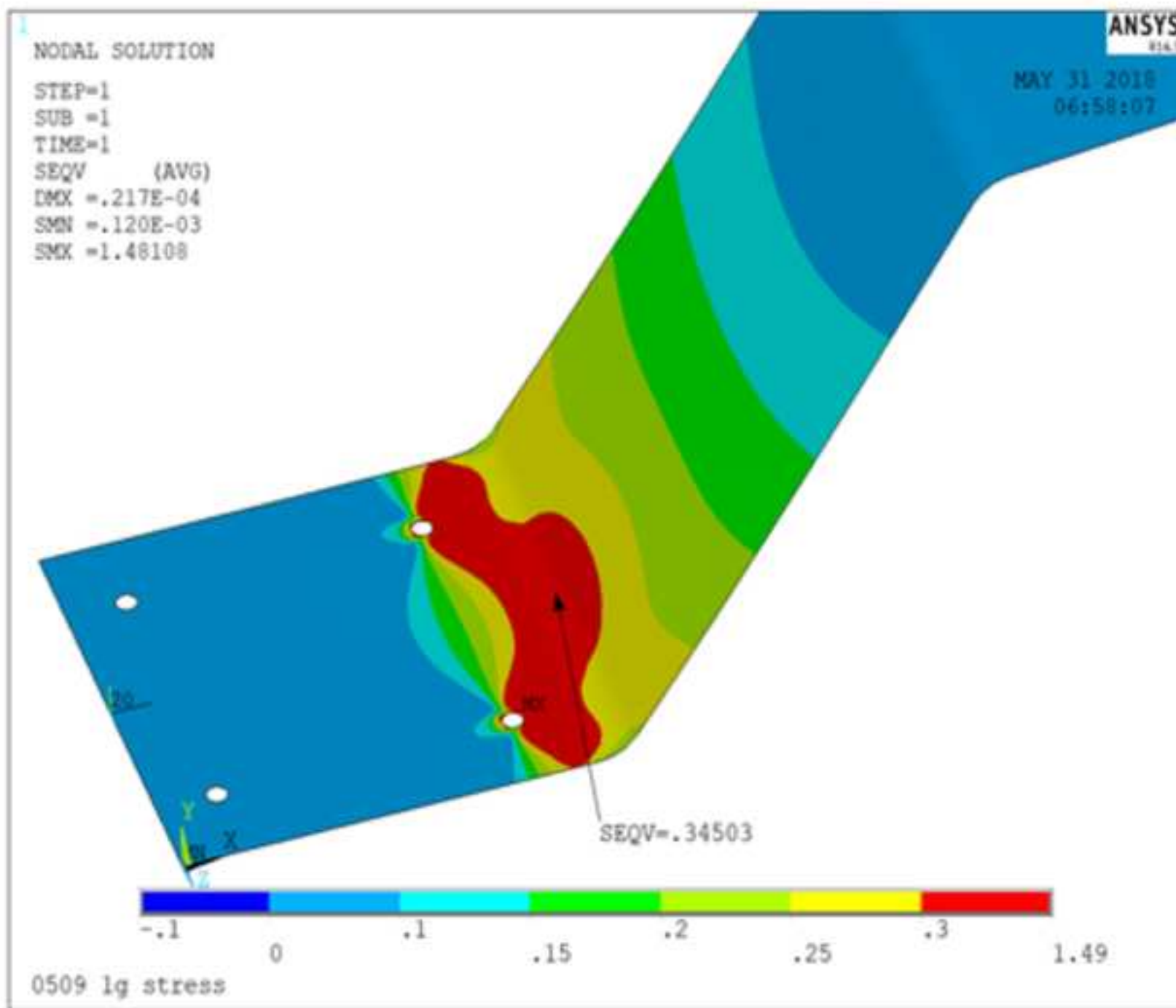
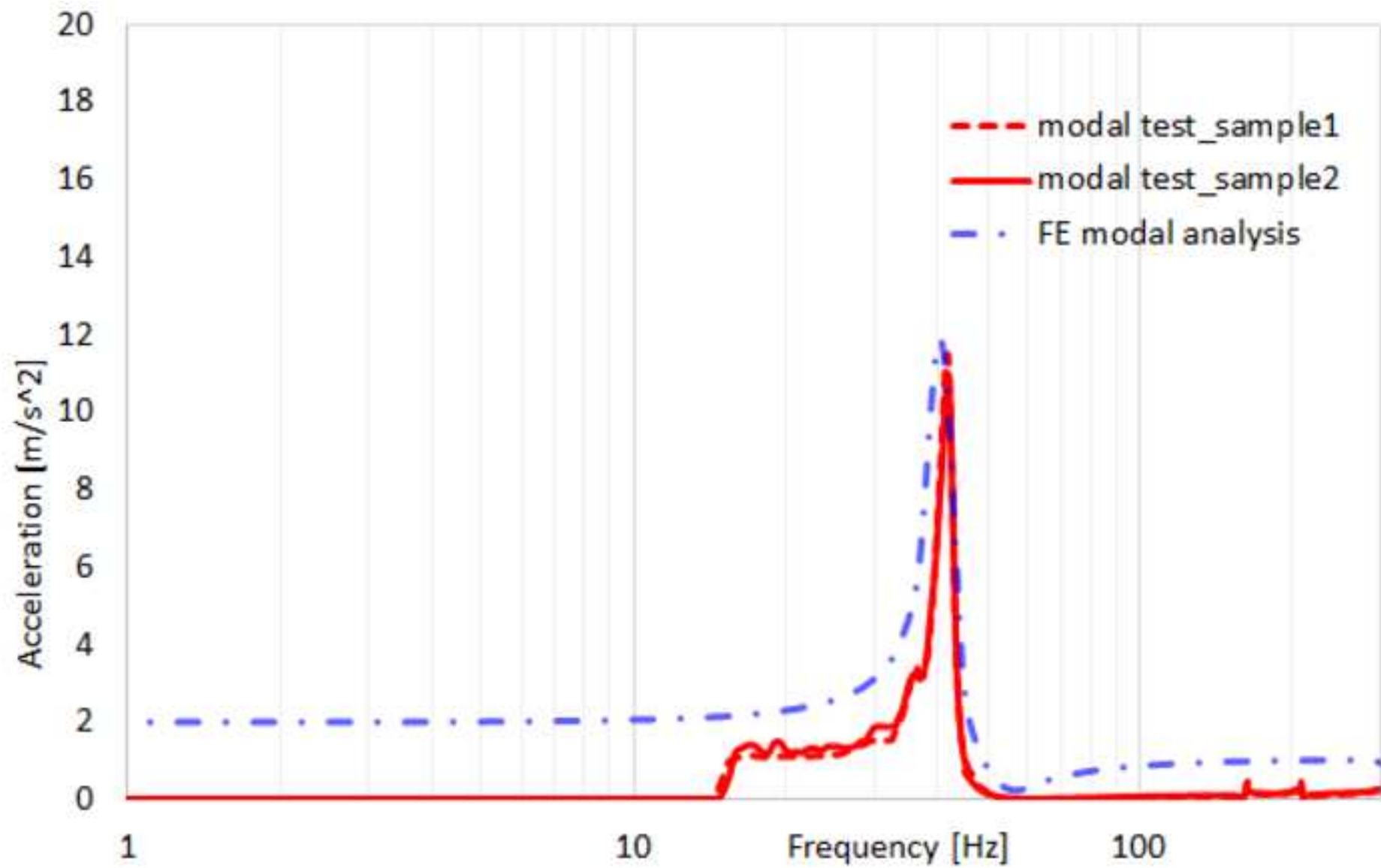
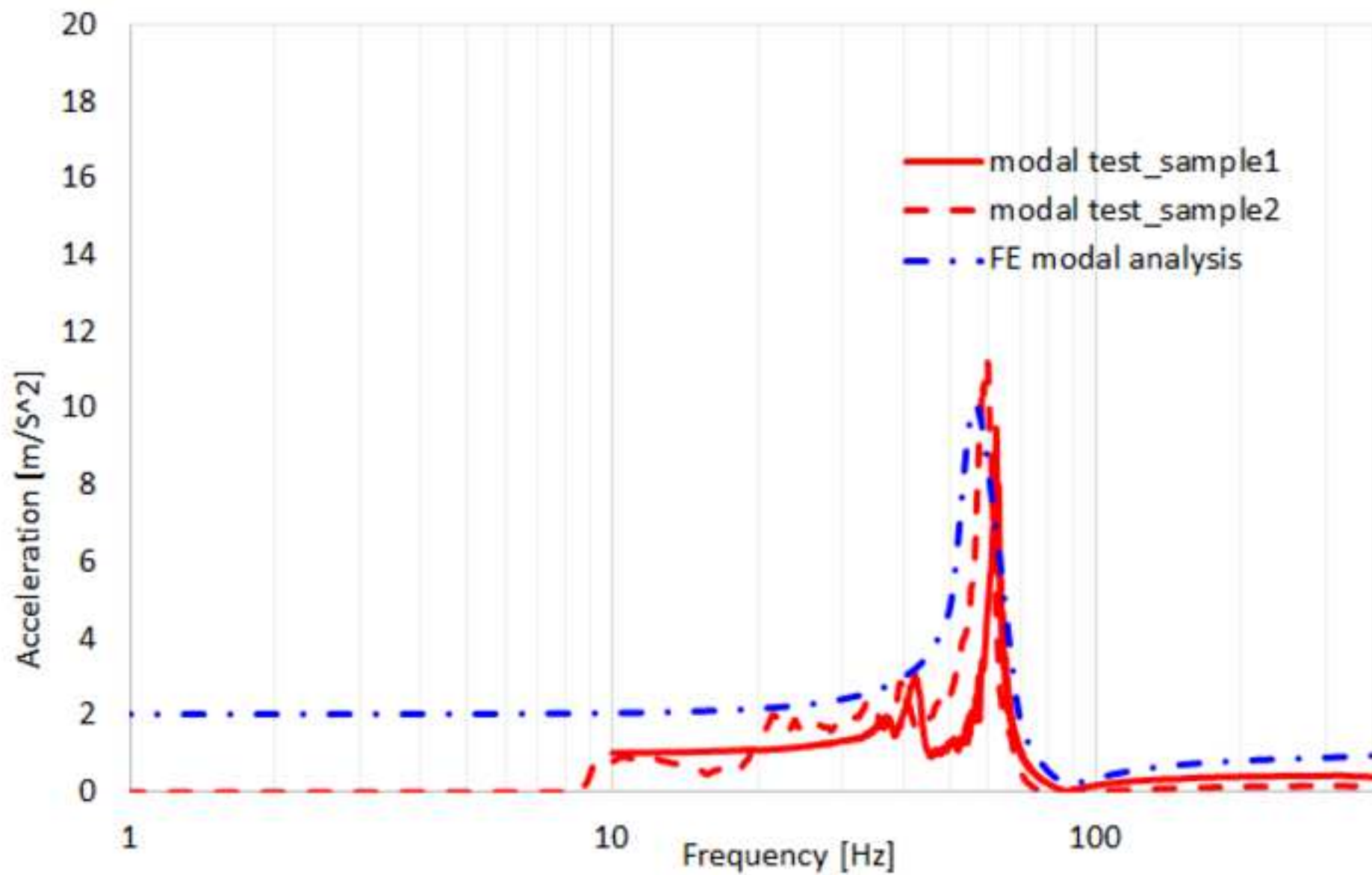
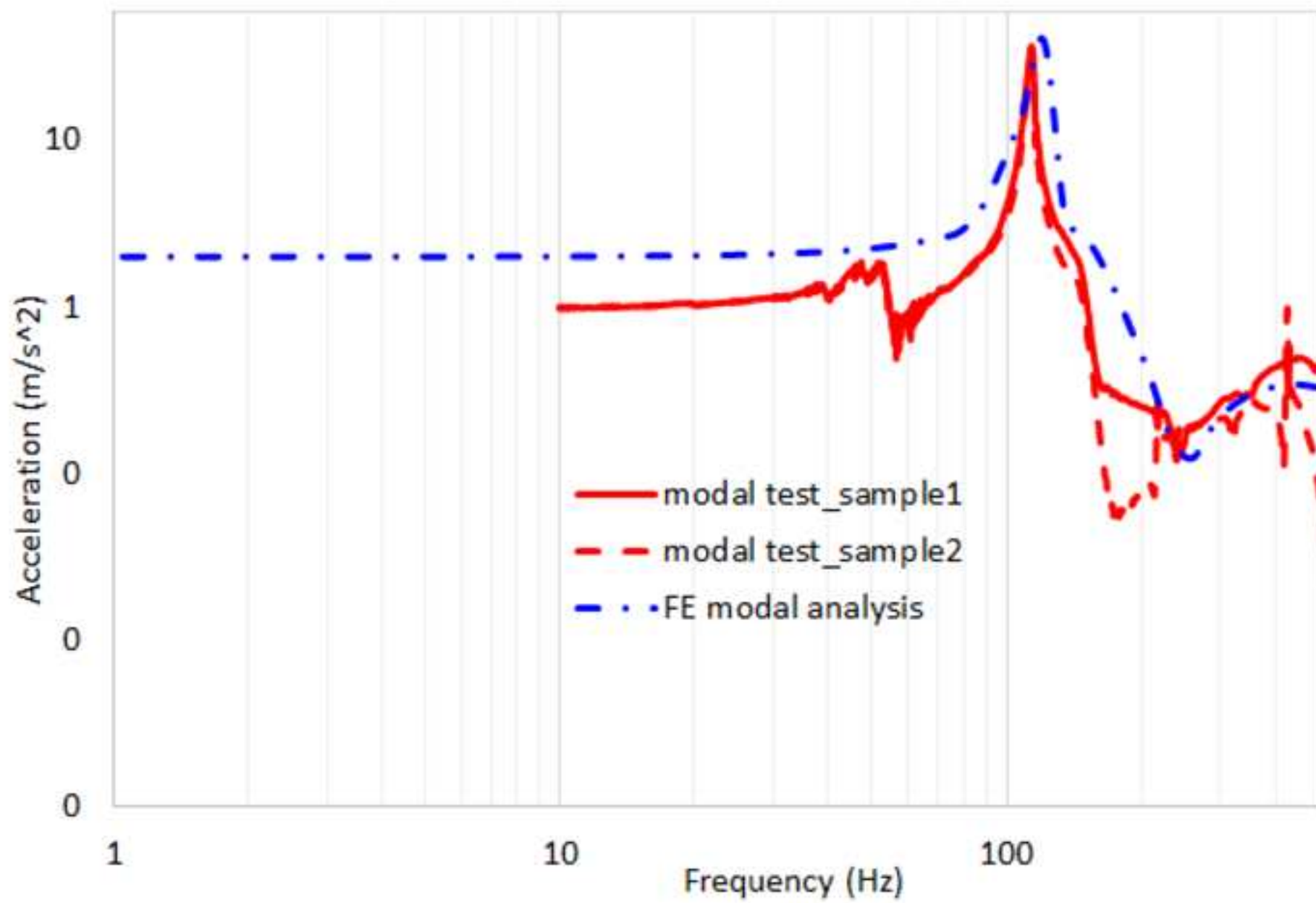


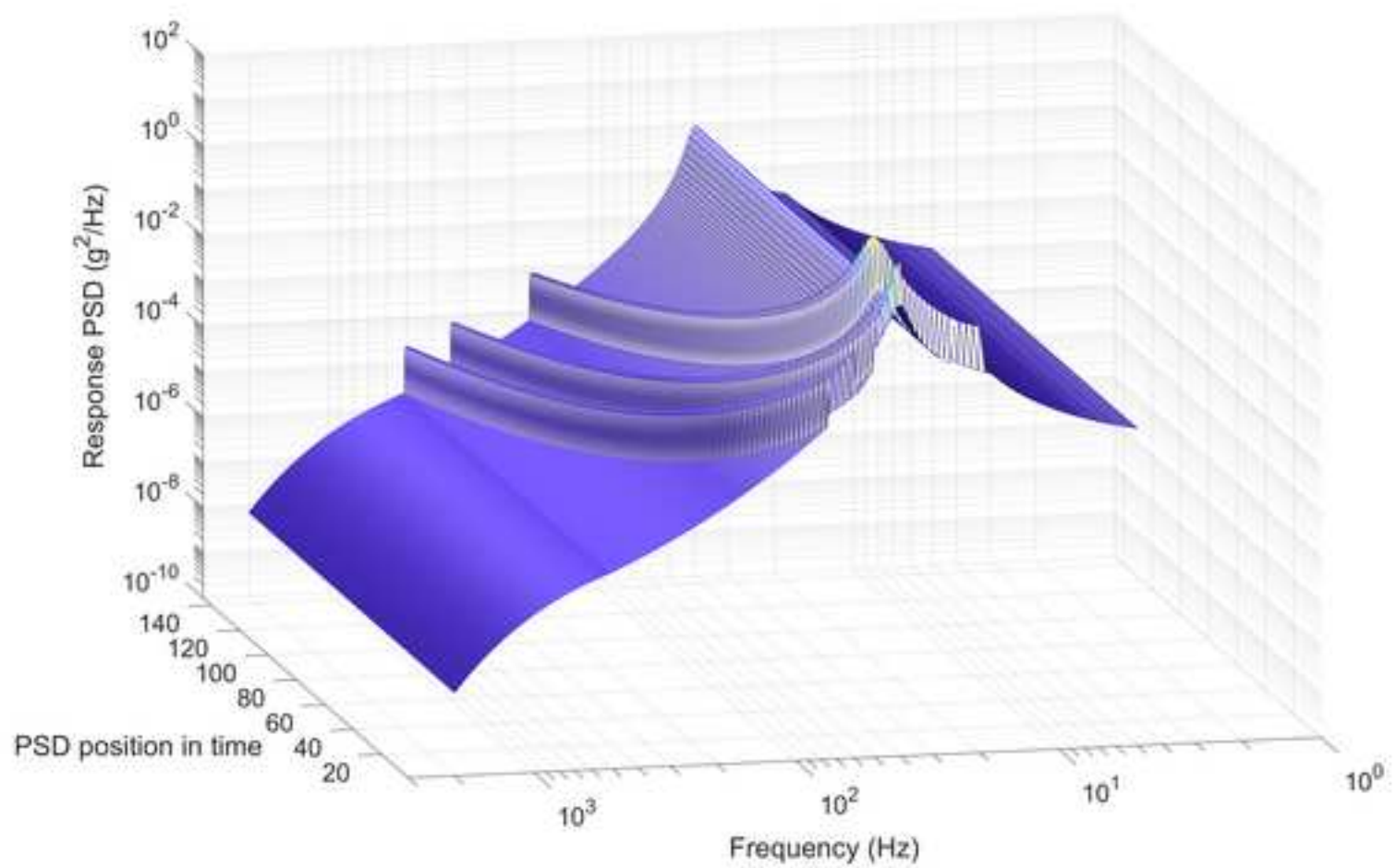
Figure 11

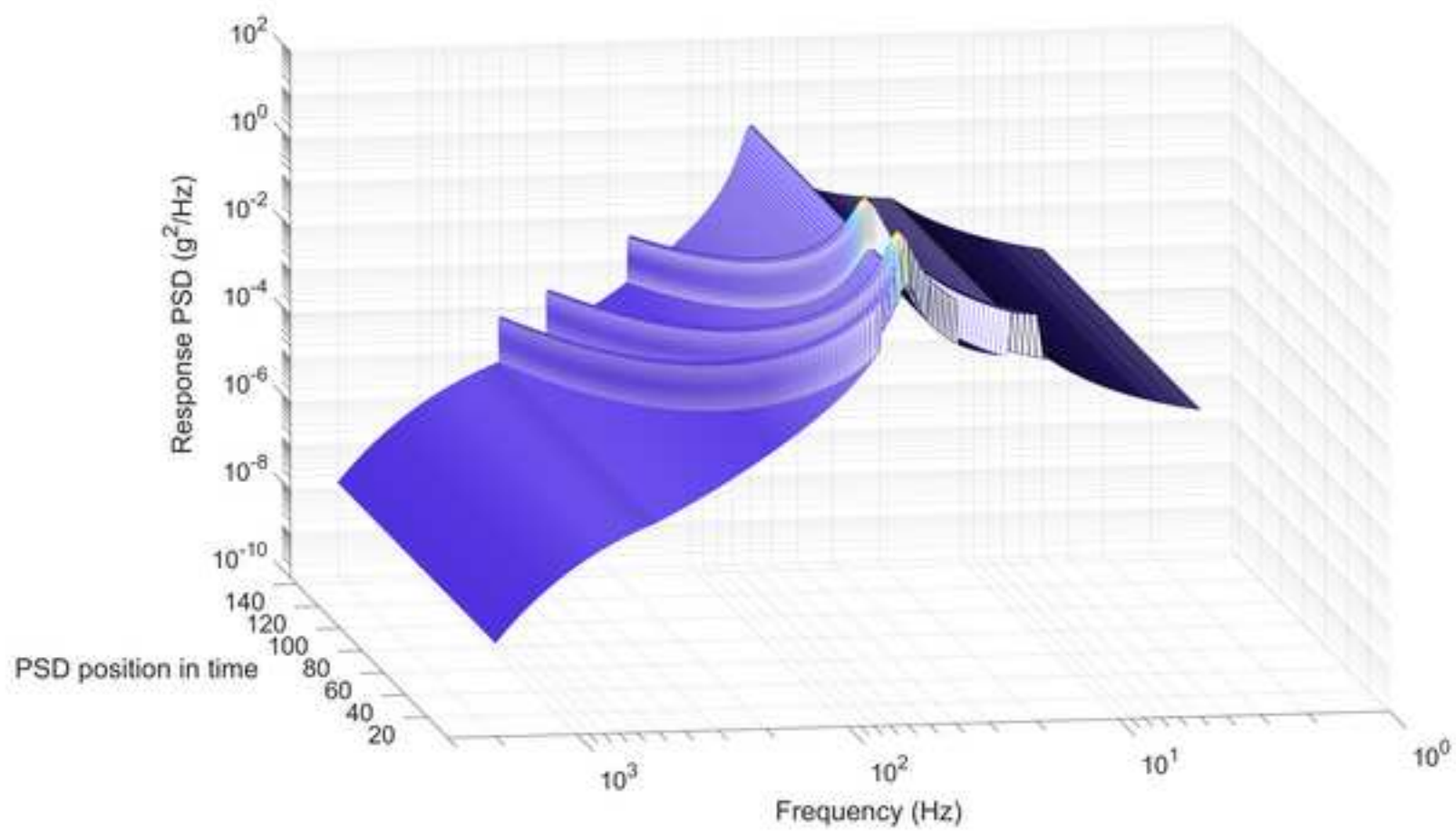












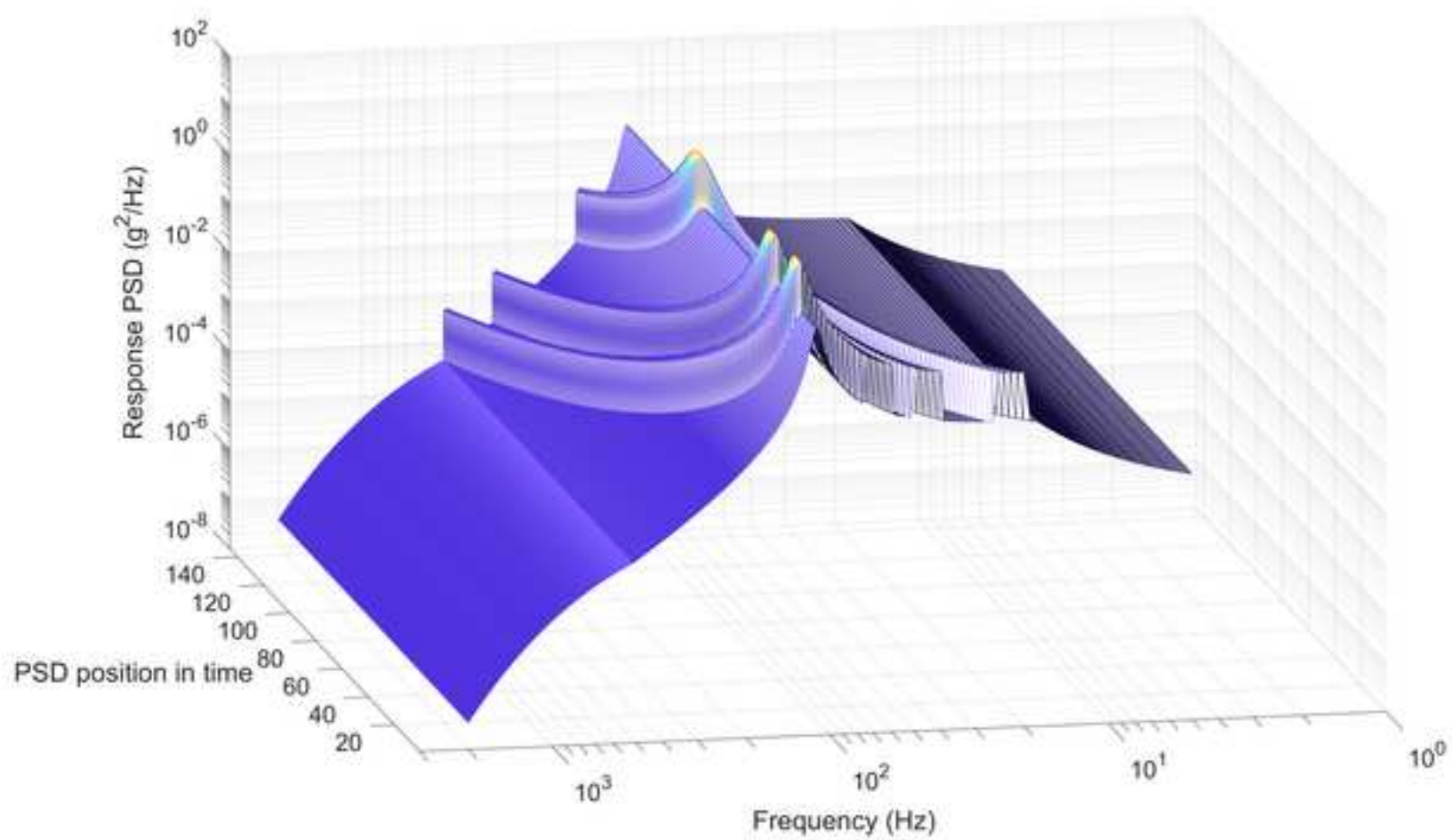
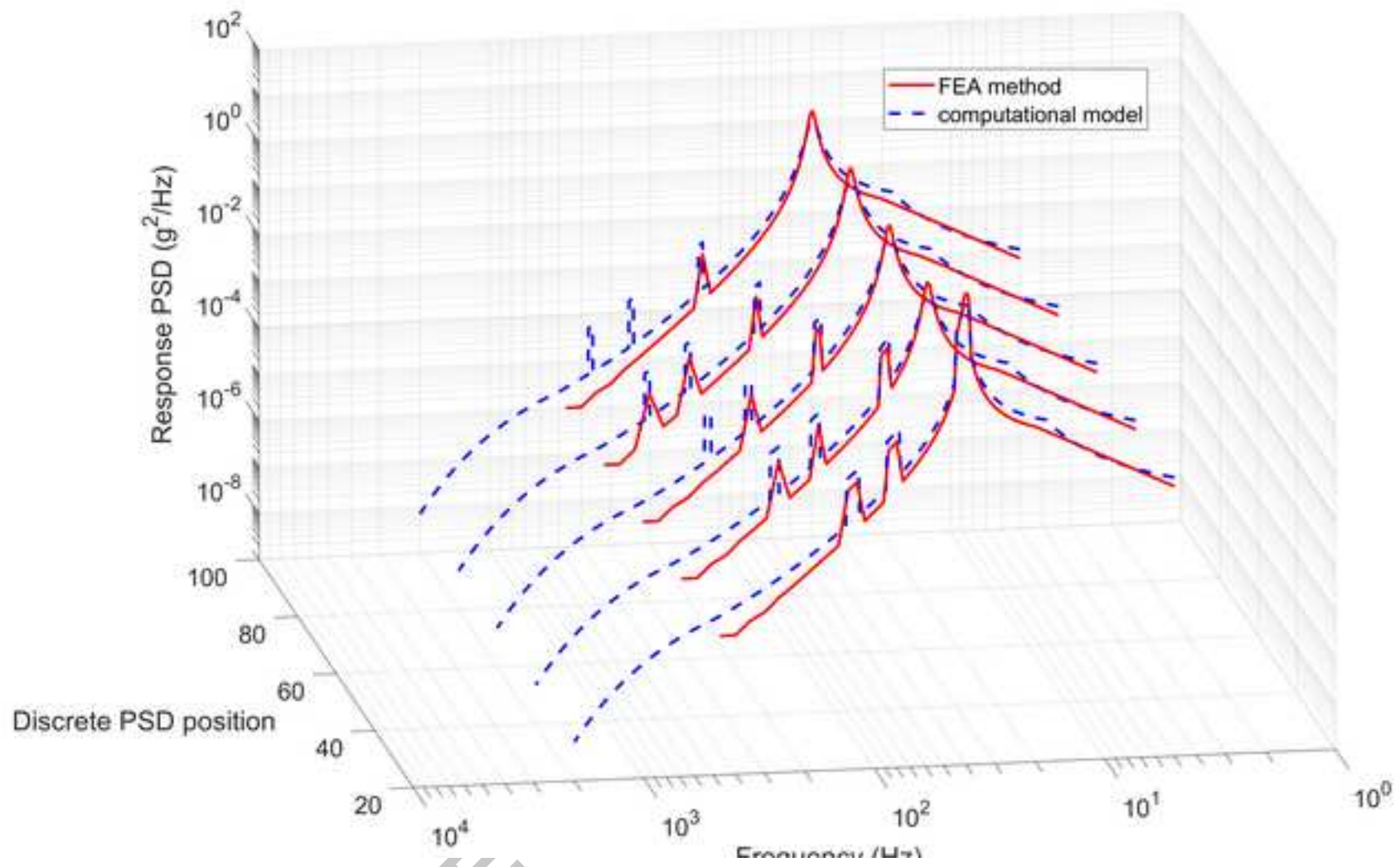
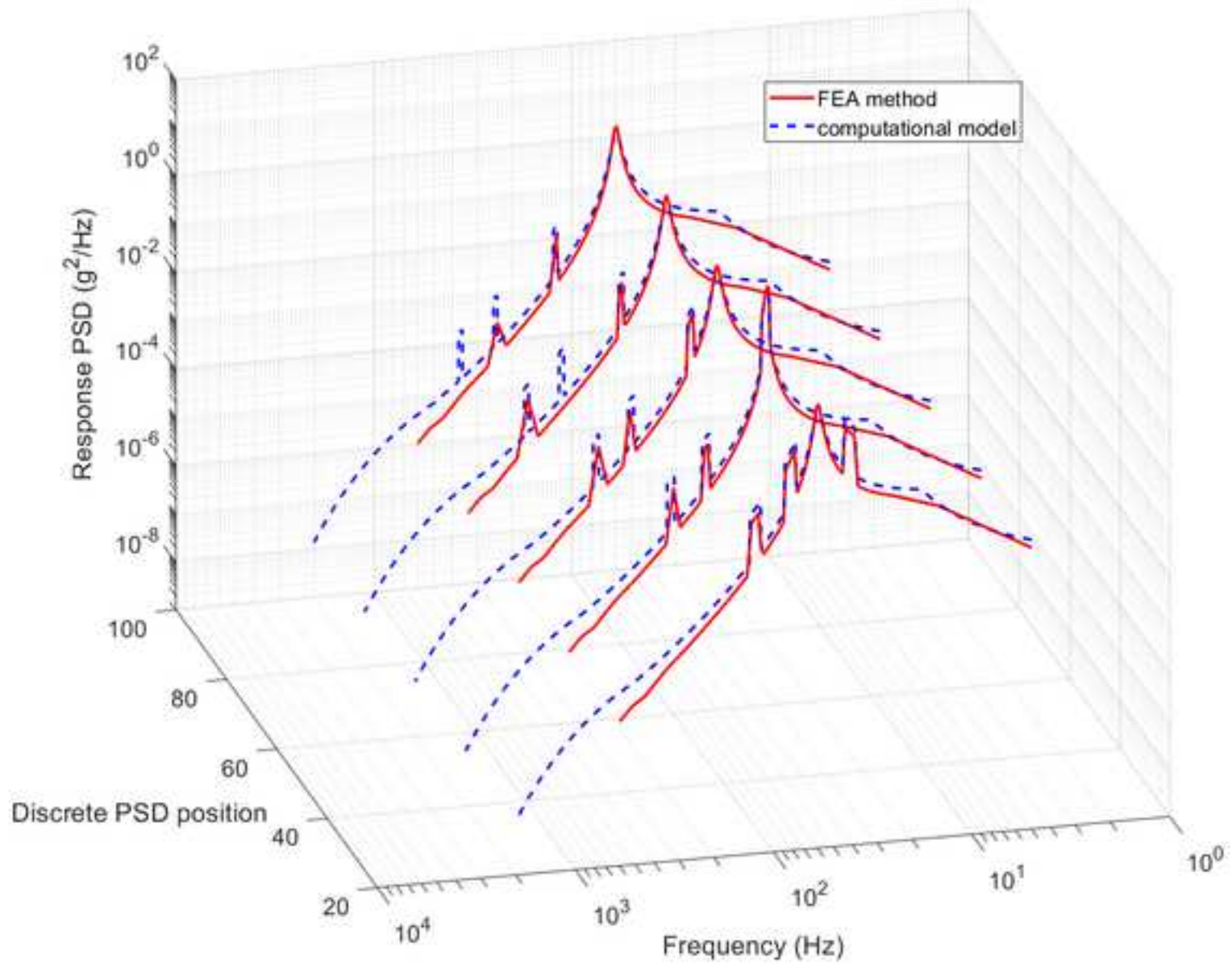


Figure 14a



ACCE

Figure 14b



ACC

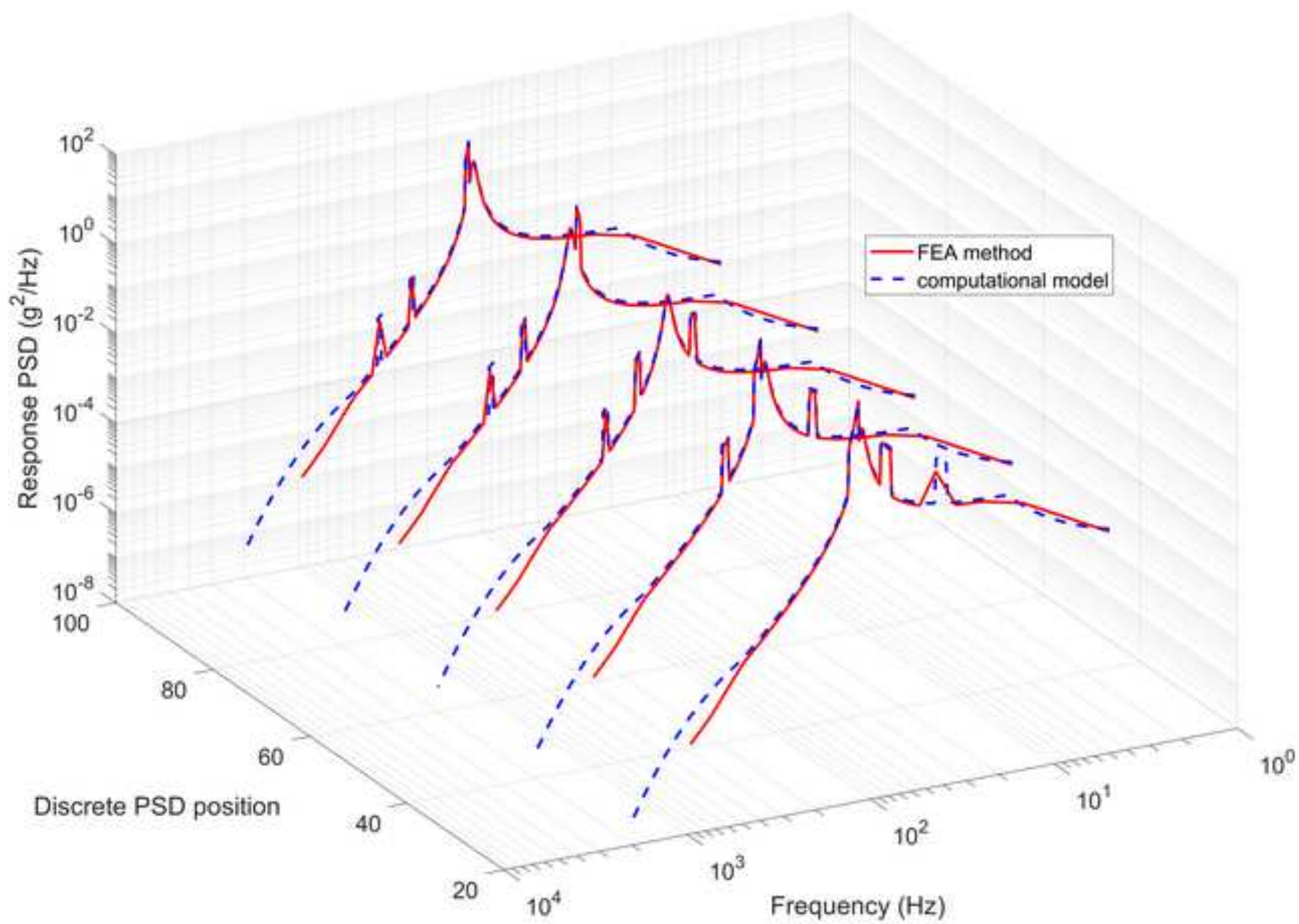


Figure 15

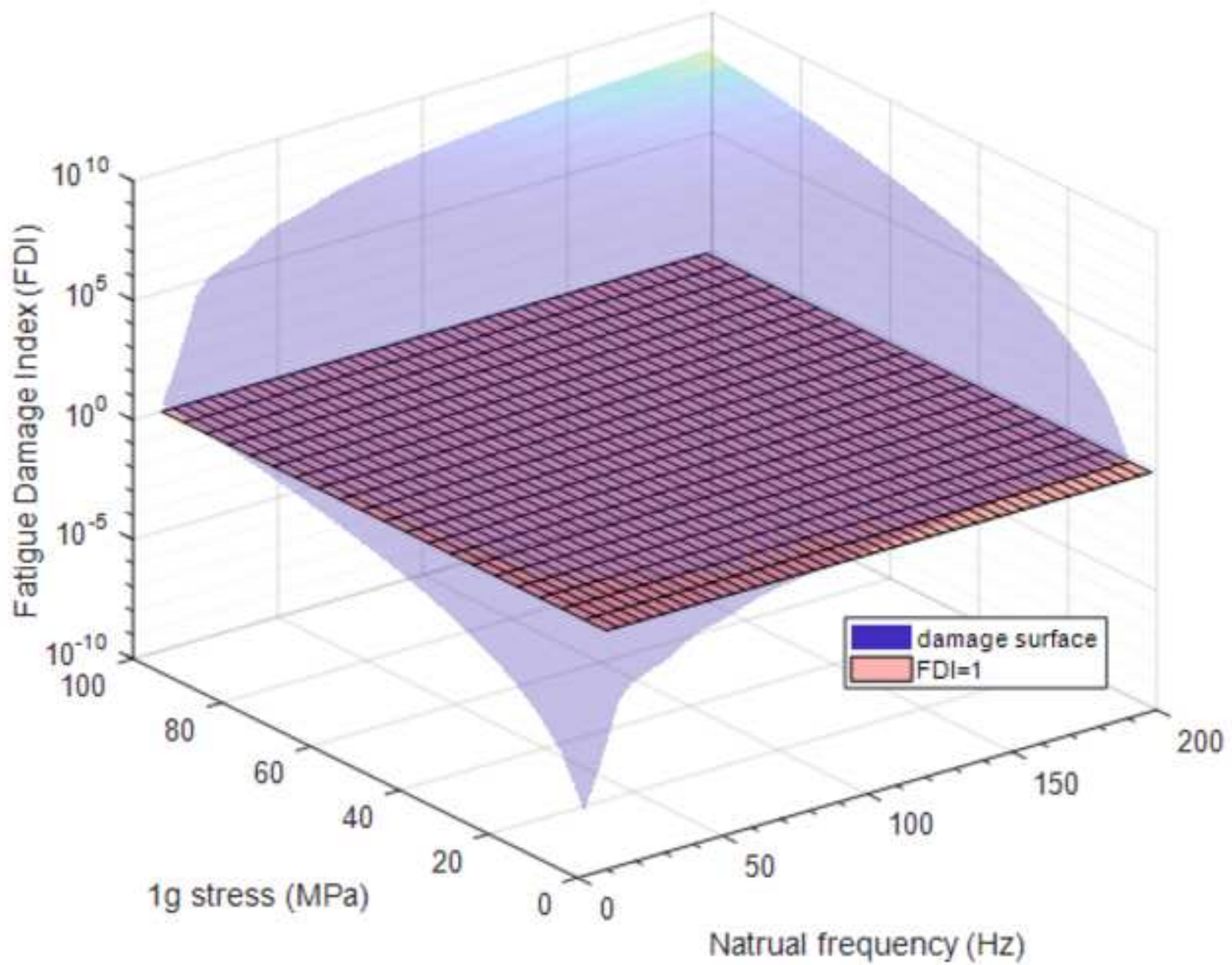


Table 1. Heavy vehicle schedule breakpoints [27]

Wideband Random Spectrum		Harmonic Swept Narrowbands			
Frequency (Hz)	Amplitude (g^2/Hz)	Narrowband	f1	f2	f3
		Bandwidth (Hz)	5	10	15
5	0.001	Swept BW (Hz)	20-170	40-340	60-510
20	0.01	Amplitude (g^2/Hz)	0.15	0.15	0.15
510	0.01	Moving rate (Hz/sec)	1	2	3
2000	0.001	# Narrowband sweep cycles	2	2	2

Table 2. Discretized stress regions of Rayleigh distribution

Centroid point for discretized stress regions	μ_1	μ_2	μ_3	μ_4	μ_5
Expected stress level, E_{μ_k}	0.64 S	1.44 S	2.35 S	3.28 S	4.23 S
Probability for each stress region, P_k	0.3935	0.4712	0.1242	0.0108	0.0003

Table 3. Material Properties of Aluminum 5052-H32

<i>Monotonic properties</i>	
Yield strength	193 MPa
Ultimate strength	228 MPa
Modulus of elasticity	70.3 GPa
Elastic Poisson's ratio	0.33
Density	2.68 g/mm ³
<i>Cyclic properties</i>	
Material constant of S-N curve, C	1348 MPa
Slope of S-N curve, b	-0.17

Table 4. Mesh properties of FE model

Mesh property	Value
Element type	Shell 63
Mesh size (mm)	3
Element number	4,104
Node number	4,311

ACCEPTED MANUSCRIPT

Table 5. FE 1G static and modal analysis

<i>Sample bracket</i>	<i>40 Hz</i>	<i>60 Hz</i>	<i>112 Hz</i>
1G von Mises stress, S_{1G} (MPa)	2.070	0.973	0.345
FE modal analysis (Hz)	40.4	58.1	113.5

Table 6. Natural frequency comparison between modal test and FE modal analysis

<i>Modal results</i>			
Modal test (Hz)	40.5	58.5	113.5
FE modal analysis (Hz)	42.6	60.8	121.0
Error (%)	5.2	3.9	6.6

Table 7. FDI comparison between the model and FEA

<i>Natural frequency of</i>	<i>40 Hz</i>	<i>60 Hz</i>	<i>112 Hz</i>
FEA method	$1.76 \cdot 10^{-6}$	$1.67 \cdot 10^{-7}$	$6.56 \cdot 10^{-9}$
Computational model	$1.23 \cdot 10^{-6}$	$1.31 \cdot 10^{-7}$	$6.88 \cdot 10^{-9}$
Error (%) for FDI	43.79%	27.13%	-4.65%

Research Highlights:

- A new fatigue damage modeling approach is proposed to predict fatigue damage of structures under complex evolutionary power spectral density (PSD) loadings where the topology of PSD function changes with time.
- The proposed approach is based on the assumption that time-varying response PSD function can be transformed into discrete PSDs and each discrete PSD can be split into narrow frequency bands so that stress spectrum can be associated with a Rayleigh distribution of stress cycles.
- The proposed modeling approach is numerically and experimentally validated by a finite element method and experiments using three simplified structures made of 5052-H32 aluminum alloy.
- The proposed modeling approach provides a more efficient modeling technique, accurately account for complex random loadings and thus give more accurate fatigue life assessment of engineering structural components.

Graphical abstract

$$\text{Total Damage Accumulation } D = \sum_{i=1}^M \sum_{j=1}^K \sum_{k=1}^L \frac{n_{i,j,k}}{N_{i,j,k}}$$

